

Politecnico di Bari

Repository Istituzionale dei Prodotti della Ricerca del Politecnico di Bari

Slope instability processes in intensely fissured clays: case histories in the Southern Apennines

This is a post print of the following article

Original Citation:
Slope instability processes in intensely fissured clays: case histories in the Southern Apennines / Cotecchia, F., Vitone, C., Santaloia, F., Pedone, G., Bottiglieri, O.. - In: LANDSLIDES. - ISSN 1612-510X. - 12:5(2015), pp. 877-893. [10.1007/s10346-014-0516-7]

Availability:
This version is available at http://hdl.handle.net/11589/1394 since: 2022-06-22

Published version
DOI:10.1007/s10346-014-0516-7

Publisher:

Terms of use:

(Article begins on next page)

17 November 2026

Landslides

SLOPE INSTABILITY PROCESSES IN INTENSELY FISSURED CLAYS: CASE HISTORIES IN THE SOUTHERN APENNINES

--Manuscript Draft--

Manuscript Number:	LASL-794R2
Full Title:	SLOPE INSTABILITY PROCESSES IN INTENSELY FISSURED CLAYS: CASE HISTORIES IN THE SOUTHERN APENNINES
Article Type:	Original Paper
Corresponding Author:	CLAUDIA VITONE BARI, ITALY
Corresponding Author Secondary Information:	
Corresponding Author's Institution:	
Corresponding Author's Secondary Institution:	
First Author:	FEDERICA COTECCHIA
First Author Secondary Information:	
Order of Authors:	FEDERICA COTECCHIA
	CLAUDIA VITONE
	FRANCESCA SANTALOIA
	GIUSEPPE PEDONE
	OSVALDO BOTTIGLIERI
Order of Authors Secondary Information:	
Abstract:	In slopes formed by tectonized clayey turbidites, the soil fissuring recurrently influences the hydro-mechanical soil properties, determining an impoverishment in strength and an increase in permeability of the slope, that make them predisposing factors of landsliding. This paper presents three case histories of slopes within tectonized clayey turbidites that are representative of several others in the Southern Apennines and, more widely, in the southern Mediterranean. The paper reports a novel attempt to connect tightly the slope geomorphological and hydro-mechanical features to the slope geological history, through an introductory presentation of the geological setting and history of the chain where the slopes occur. The slopes, location of very slow landslides, have been reconstructed based upon field surveys and investigations, multi-aerial photo-interpretation, laboratory testing, monitoring and numerical modelling. Furthermore, novel is the attempt to present, all together, the behaviour of the soils involved in the three landslide case studies, in the light of the mechanical modelling approach to fissured clays recently presented in the literature.

Powered by Editorial Manager® and ProduXion Manager® from Aries Systems Corporation

Manuscript
Click here to download Manuscript: Text_Cotecchia et al_2nd_Revision .docx
Click here to view linked References

SLOPE INSTABILITY PROCESSES IN INTENSELY FISSURED CLAYS: CASE HISTORIES IN THE SOUTHERN APENNINES

Federica Cotecchia*, Claudia Vitone*, Francesca Santaloia°, Giuseppe Pedone* and Osvaldo Bottiglieri*
* Technical University of Bari, Bari, ITALY
° IRPI-CNR, U.O.S. Bari, ITALY

Federica Cotecchia, PhD, full professor

federica.cotecchia@poliba.it

Claudia Vitone, PhD, lecturer

claudia.vitone@poliba.it

Francesca Santaloia, PhD, lecturer

f.santaloia@ba.irpi.cnr.it

Giuseppe Pedone, PhD

giuseppe.pedone@poliba.it

Osvaldo Bottiglieri, PhD

osvaldo.bottiglieri@poliba.it

Corresponding author:

Claudia Vitone, Technical University of Bari, Bari, Italy

email: claudia.vitone@poliba.it

tel. (+39)3391610977

NOTATION LIST

A Activity
A-B-C: source, channel and accumulation zones of Vadoncello landslides
A-C-C9-F-G-L: labels for Pisciolo landslide bodies
A-F *in-situ* soil complexes within Vadoncello slope
BENT bentonite clay
c' cohesion intercept
CF Clay Fraction
C_k permeability change index
e void ratio
FAE Faeto Flysch
F-ID Fissuring IDentity
G-I landslide soil complexes within Vadoncello slope
ICL Intrinsic Compression Line
INCL* Isotropic Normal Consolidation Line of the reconstituted clay
k_s saturated permeability
N Numidian Flysch
p' mean effective stress
p^*_e equivalent mean effective stress on the INCL*
p'_y mean effective stress at yield in isotropic compression
PD Paola Doce Formation
PD1 lower unit of Paola Doce Formation
PD2 upper unit of Paola Doce Formation
PI Pisciolo hillslope
PI Plasticity Index
R overconsolidation ratio: p'_y / p'
REV Representative Element Volume
RF Red Flysch
SBS State Boundary Surface of natural clay
SBS* State Boundary Surface of reconstituted clay
SCM Santa Croce di Magliano slopes
SEN Vadoncello slope
SF Sand Fraction
S_σ stress sensitivity ratio: p'_y / p^*_e
USCS Unified Soil Classification System
ν specific volume
ε_v^p plastic volumetric strain
ϕ_{cs}^* critical state friction angle of the reconstituted clay
ϕ'_{cs} critical state friction angle of the natural clay
ϕ'_m mobilised friction angle
ϕ'_{peak} friction angle at peak for natural clay
$\phi'_{post-peak}$ friction angle at post-peak for natural clay
ϕ'_r residual friction angle

SLOPE INSTABILITY PROCESSES IN INTENSELY FISSURED CLAYS: CASE HISTORIES IN THE SOUTHERN APENNINES

F. Cotecchia*, C. Vitone*, F. Santaloia°, G. Pedone* and O. Bottiglieri*

* Technical University of Bari, Bari, ITALY

° IRPI-CNR, U.O.S. Bari, ITALY

ABSTRACT

In slopes formed by tectonized clayey turbidites, the soil fissuring recurrently influences the hydro-mechanical soil properties, determining an impoverishment in strength and an increase in permeability of the slope, that make them predisposing factors of landsliding. This paper presents three case histories of slopes within tectonized clayey turbidites that are representative of several others in the Southern Apennines and, more widely, in the southern Mediterranean. The paper reports a novel attempt to connect tightly the slope geomorphological and hydro-mechanical features to the slope geological history, through an introductory presentation of the geological setting and history of the chain where the slopes occur. The slopes, location of very slow landslides, have been reconstructed based upon field surveys and investigations, multi-aerial photo-interpretation, laboratory testing, monitoring and numerical modelling. Furthermore, novel is the attempt to present, all together, the behaviour of the soils involved in the three landslide case studies, in the light of the mechanical modelling approach to fissured clays recently presented in the literature.

KEYWORDS: fissured clays, slow landslides, mechanical and hydraulic soil properties, tectonized flysch

INTRODUCTION

The soils outcropping within chain areas, namely areas that have been location of orogenesis, have generally experienced severe tectonic processes. This is the case of the soils within the Apennines in southern Italy, a chain area part of one of the most important and still active thrust systems in the Mediterranean. The present paper focuses on instability processes that recur in tectonized clay slopes across this chain and on the slope factors predisposing to instability.

The tectonized soil sequences are classified, since the seventies, as "structurally complex formations" (e.g., Croce 1971; AGI 1979), due to their lithological variability, heterogeneous consistency and fissuring. Several research studies (Croce 1971; Pellegrino and Picarelli 1982; Fenelli et al. 1982; Santaloia et al. 2001; Cotecchia et al. 2007) have shown that the soils part of structurally complex formations exhibit very low shear strength, by comparison with that of soils of the same composition, but possessing a structure that has not experienced severe disturbance due to tectonics. Consequently, the poor shear strength of the tectonized soils represents a common internal factor (Terzaghi 1950) predisposing the slopes to failure in the area of reference in the present paper. Hence, the mechanical characterisation of the tectonized soils is crucial for landslide hazard assessments.

The inhomogeneities and the fissuring of tectonized soils introduce critical difficulties in both investigation and interpretation of their behaviour (e.g., Calabresi and Manfredini 1973; Cicolella and Picarelli 1990; Cotecchia and Santaloia 2003; Picarelli and Olivares 2004; Airò Farulla et al. 2010). Overcoming these difficulties has been the goal of a research carried out at the Technical University of Bari, aimed in particular at characterising the influence of fissuring on the hydro-mechanical properties of tectonized clays (Cotecchia and Santaloia 2003; Cotecchia and Vitone 2011; Vitone and Cotecchia 2011; Vitone et al. 2013a, b). In this paper, the main results of the research are recalled, first to show how the basic features of the hydro-mechanics of fissured clays can be modelled by means of a single framework. As second, it is shown how this framework proves that the hydro-mechanical properties of fissured clays can predispose slopes to failure.

In particular, they are discussed the properties of the tectonized clays present in Southern Apennine slopes that are location of very slow landslides, together with the corresponding landslide mechanisms. These have been reconstructed based upon field surveys and investigations, multi-aerial photo-interpretation, laboratory testing, monitoring and numerical modelling. The chosen slopes are representative of several others in the Southern

Apennines. They are (Fig. 1): the Vadoncello slope (western sector of the chain), located down the Senerchia village in the upper Sele River Valley; the Pisciolo hillslope, located on the right side of the Ofanto River valley, to the West of Melfi (eastern sector of the chain); the Santa Croce di Magliano slopes (eastern sector of the chain).

As first, the paper reports a presentation of the geological setting and history of the chain, in order to connect tightly the current slope geomorphological and hydro-mechanical features to the slope history. Thereafter, the paper reports a novel attempt to show how the behaviour of all the soils involved in the three landslide case studies fits the mechanical modelling cited before. In a wider perspective, the aim of the work is to contribute to the characterisation of the possible landslide mechanisms occurring in landscapes ensued from an intense tectonic history. These landscapes are recurrent in the southern Mediterranean, where landsliding is very diffuse and represents a major problem for socio-economic development.

GEOLOGICAL SETTING

The Italian Southern Apennine is part of the Apennine-Maghrebian chain, important branch of the circum-Mediterranean Alpidic system (Fig. 1). It is a Neogene to Quaternary thrust belt, verging to North-East, located in the hanging wall of a West-directed subduction of the Adriatic-African lithosphere, under the European plate (Malinverno and Ryan 1986; Doglioni 1991). It is bordered, to the East, by the Pliocene-Pleistocene foredeep (Bradano Through) and, to the West, by the Tyrrhenian back-arch basin (Scrocca et al. 2005; Fig. 1).

In particular, the Southern Apennine allochthonous nappes derive from the deformation of basin and platform domains within the passive margin of the Adriatic-African plate (Patacca and Scandone 2007). The geological literature does not provide a single conclusive interpretation of the paleogeographic setting of such passive margin and several evolution models have been proposed (Scrocca et al. 2005). The stratigraphic and structural origin of the slopes under study seem to be best represented by the model shown in Fig. 2 (Ogniben 1969; Pescatore et al. 1999). According to it, the main Mesozoic domains involved in the tectonic evolution were, from the West to the East: the Liguride-Sicilide marine domain of the Liguria-Piedmont Ocean, the Apennine carbonate platform, the Lagonegro-Molise marine basin and the Apulian carbonate platform (Fig. 2a). This paleogeographic setting has evolved since Paleogene, as a consequence of the onset of the Apennine orogenesis (Dewey et al. 1989). The internal sectors of the Lagonegro-Molise basin were piled up into the Apennine chain, during Late Oligocene-Early Miocene, while, to the East, turbiditic and hemipelagic successions were deposited in the Irpinian basin (Fig. 2b, Pescatore and Senatore

1986). These successions were thereafter involved in the piling up (Late Miocene) of the Southern Apennine accretionary prism (Fig. 2; Di Nocera et al. 2006).

As a consequence, the geological units (Fig. 2c) deposited in the internal domain, i.e., the Sicilide Unit, occur in the highest portions of the chain, moving further away from its depositional realm, while those formed in the Irpinian basin, i.e., the Daunia Unit, are located in the lowest and easternmost portion of the chain (Patacca and Scandone 2007). Fig. 2c shows two schematic geological sections and the location of the slopes under study: the Vadoncello slope, SEN, the Pisciolo hillslope, PI, and the Santa Croce di Magliano slopes, SCM.

The soils forming the SEN slopes are turbidites belonging to the Sicilide Unit (Fig. 2). The turbiditic sequences outcropping at PI, part of the Fortore Unit, were formed within the northern sector of the pre-orogenic Lagonegro-Molise basin. The clay-rock sequences at SCM belong to the Daunia Unit, formed in the Irpinian basin (Fig. 2). After their deposition, all these sedimentary successions were folded and faulted during orogenesis and, thereafter, were involved in neotectonic events, often giving rise to disarrayed and fissured clay-rock masses.

In more detail, the SEN soils are varicoloured intensely fissured clays part of the allochthonous Variegated Clay Formation (Upper Cretaceous-Lower Miocene); they are chaotically interbedded with fractured rock masses. The geological map and section of the Vadoncello slope are shown in Fig. 3 and will be discussed later in some detail. The clays are in lateral contact with karst calcareous rocks of the Picentini Mountains (Apennine platform in Fig. 2a), that host an important aquifer (Fig. 4).

Clays and isolated rock masses part of the Paola Doce Formation (PD hereafter; Late Oligocene-Lower Miocene) crop out on the PI hillslope, whose geological map and sections are shown in Fig. 5. This formation overlies the Red Flysch (RF herein) and is locally overlain by the Numidian Flysch (N in the following). The clays are found laminated and fissured, including disarranged rock levels from centimetres to metres thick. As depicted in Fig. 5, two different units, PD1 and PD2, have been distinguished in the PD succession, in relation to the frequency and thickness of the rock intervals and coarse layers, which increase from the lower PD1 to the upper PD2.

The clays outcropping along the SCM slopes (Fig. 6) are part of the Red Flysch (RF; Oligocene-Miocene) and are overlain by the marly limestones of the Faeto Flysch (FAE). Some bentonite layers (BENT) are found at places resting on the RF (Fig. 6).

The brief outline of the geological setting of the slopes under study (Fig. 1) reveals that the interbedding of fractured rock strata within the fissured clays is a common slope feature. The geotechnical characterisation of the three

sites, discussed later in the paper, focused mainly on the clay properties, since these represent the weakest and most diffuse lithotype, that controls the slope stability.

HYDRO-MECHANICAL BEHAVIOUR OF THE CLAYS FORMING THE SLOPES

A framework of behaviour for fissured clays

The characterisation of fissured clays has always been a major task for geotechnical research (Terzaghi 1936; Lo 1970; AGI 1979; Cicolella and Picarelli 1990; Marsland 1971; Petley 1984; Fearon and Coop 2000, 2002; Picarelli and Olivares 2004; Hight et al. 2007; Silvestri et al. 2007; Airò Farulla et al. 2010). Recent research has been carried out with the aim of assessing a basic simple framework of the influence of fissuring on the mechanics of clays (e.g., Cotecchia and Santaloia 2003; Vitone 2005; Cotecchia et al. 2007; Cotecchia and Vitone 2011; Vitone and Cotecchia 2011), to be addressed in practice for the prediction of the strength reduction stemming from fissuring. The fissuring features have been codified by means of the characterisation chart in Fig. 7, which accounts for both the lithology and consistency of the soil matrix (categories A and B) and the discontinuity features: fissuring nature (C, D, E), orientation (F) and geometry (G-H-I). Fissuring intensity can be characterised by either the average volume of the clay elements between the fissures (i.e., their bulk dimension), or by their specific surface, i.e., average area of the clay element per unit volume. Through several testing programmes on different clays it has resulted that the categories that influence most the fissured clay behaviour are both the fissuring orientation (from single, F1, to random, F3) and the intensity (I).

The applicability of continuum mechanics and element testing to characterise the mechanics of clays of fissuring intensity from I6 to I4, has been verified by means of full field measurements, using either the False Relief Stereophotogrammetry method (Desrues and Viggiani 2004; Vitone et al. 2009), or Digital Image Correlation techniques (Vitone et al. 2012, 2013 a, b). These measurements have shown that, within Representative Element Volumes (REV) of I4-I6 clay, with fissuring orientation either F3, or F1/0°-30° (fissure inclination with respect to the horizontal and minimum principal stress), the development of shear bands across the specimen takes place similarly to what observed for unfissured clays. Therefore, for these fissure identities (F-IDs hereafter, see Fig. 7), the element test data can be used according to traditional soil mechanics, as for unfissured clays. For F1/30°-90°, instead, strain localization takes place since small displacements and is controlled by pre-existing fissures, which dominate the response of the specimen and make it far weaker. Hence, the characterisation of fissured clay mechanics may be

formalized using continuum mechanics, but, for F3 and F1/0°-30°, it must be developed with reference to REVs which depend on the F-ID, whereas for F1/30°-90°, the element size is irrelevant and the model must account for a significant strength decrease (strength anisotropy; Vitone et al. 2013 a, b).

The behaviour of fissured clays (of F-IDs indicated in grey in Fig. 7; data from Fearon and Coop 2000, 2002; Cotecchia and Santaloia 2003; Cicolella and Picarelli 1990; Vitone and Cotecchia 2011) has been compared with that of the same clays when reconstituted in the laboratory (Burland 1990; Cotecchia and Chandler 2000) and that of unfissured structured clays (Vitone and Cotecchia 2011; Cotecchia and Vitone 2011). Among these, the reconstituted clay possesses the weakest micro-structure. The framework resulting from this comparison is sketched in Fig. 8, where Fig. 8a refers to compression and Fig. 8b to shear. The compression curve of the fissured clay is found to lie on the left of the Intrinsic Compression Line (ICL, Burland 1990) of the reconstituted clay up to high pressures. Hence, the fissured clay does not enter the so-called structure permitted space (Leroueil and Vaughan 1990), possible only for sensitive unfissured clays (Fig. 8a). Cotecchia and Chandler (2000) introduced, for unfissured clays, the stress sensitivity ratio, $S_\sigma = p'_y / p^*_e$ (ratio between the mean effective stress at gross yield in isotropic compression, p'_y, and the equivalent pressure on the isotropic normal consolidation line of the reconstituted clay, p^*_e) to quantify the influence of microstructure on the clay gross yielding. Gross is referred to distinguish, from the first yielding, that followed by major plastic straining and occurring about the state boundary surface (Cotecchia and Chandler 2000). S_σ has resulted to be ≥ 1 for unfissured sensitive clays. This finding implies that the natural microstructure may provide the clay with a larger state boundary surface and larger strength with respect to the reconstituted. Fig. 8a shows, instead, that for clays of whatever microstructure, but whose mesofabric includes fissuring, $S_\sigma < 1$ (Vitone and Cotecchia 2011).

As implied by $S_\sigma < 1$, shear testing has shown that the state boundary surface, SBS, of the fissured clay is smaller than that of the reconstituted clay, SBS*, irrespective of any other F-ID feature, as shown in Fig. 8b. Hence, for fissured clays, even when the microstructure is strong with respect to that of the reconstituted, its influence on the clay mechanics is overcome by fissuring. The latter makes the clay not only weaker than the corresponding unfissured clay, but also weaker than the clay when reconstituted. Moreover, where for sensitive unfissured clays structure degradation occurs with post gross yield compression and gives rise to a negative hardening component ($dS_\sigma/d\varepsilon_v^p < 0$ where ε_v^p is the plastic volumetric strain), for fissured clays, structure strengthening post gross yield compression (Fig. 8b)

contributes to a positive hardening ($dS_\sigma/d\varepsilon_v^p>0$).

In the following, the geotechnical characterisation of the fissured clays sampled at the sites indicated in Figs 1 and 2 will make reference to the framework in Fig. 8.

The fissured clays within the slopes

Table 1 reports the F-IDs of the clays sampled within the three aforementioned slopes (Figs 1 and 2; F-IDs also in Fig. 7). With reference to the clays outcropping at PI hillslope, the data in the Table are referred separately to units PD1 and PD2.

At all the sites of reference, there exist clays of fissuring intensity I6, whose mesofabric is characterised by fissures splitting the clay into millimetre lens-shaped elements, called *scales* (AGI 1979). The mesofabric of the bentonite clays from SCM, instead, is characterised by centimetre size clay elements, i.e. fissuring intensity I5, and for some of the PI clays, fissuring intensity may be even lower, i.e. I5-I4. Also, the fissure orientation varies from single, F1, to random, F3.

Table 1 reports also the ranges of the clay index properties and initial void ratios, e_0, determined in the laboratory according to ASTM standards. The clay fraction is highest for SCM clays. Almost all the samples can be classified as CH, according to the USCS classification (Unified Soil Classification System; ASTM 1985) and are of medium (SCM and SEN scaly clays) to high activity (BENT). Their consistency is high, except for BENT clay.

As resulting from x-ray diffraction analyses, the mineralogy of the medium activity SCM and SEN clays includes large quantity of mixed-layer illite-smectite, along with some smectite. Pure smectite is dominant in BENT clay.

When reconstituted in the laboratory, the clays in Table 1 exhibit strength properties (defined as intrinsic by Burland 1990) that are rather poor, due to their high plasticity. Hence, an intrinsic slope weakness stems from the composition of the clays, which represents an internal predisposing factor of slope failure. However, since the strength properties of natural clays depend not only on composition, but also on their natural structure (Burland 1990; Cotecchia and Chandler 2000), the mechanical behaviour of the undisturbed fissured clay samples in Table 1 has been also investigated. The applicability of the behavioural framework shown in Fig. 8 to the clays has then been verified.

The oedometer compression curves of the undisturbed clay samples are shown in Fig. 9, along with the relevant ICLs. The curves confirm the framework in Fig. 8a, since for each natural fissured clay the compression curve is located on the left of the ICL. Also, as typical for fissured clays, the curve has a mild curvature, with no abrupt drop in

stiffness at any pressure. This mild curvature is probably due to the combination of progressive packing of the clay elements and the degradation of the intra-element bonding (Vitone and Cotecchia 2011). Fig. 10 shows variation in specific volume, ν, with the mean effective stress, p', experienced by BENT clay specimens during isotropic compression and undrained shear. The ν-p' data confirm $S_\sigma<1$ for fissured clays also in isotropic compression. Moreover, the contractive nature of the shear response of the specimens isotropically consolidated to ν-p' states to the left of the isotropic normal consolidation line of the reconstituted clay, INCL*, confirms that *wet* shear behaviour (Schofield and Wroth 1968) and gross yielding occur on the left of INCL*. The undrained shear state paths of BENT clay are shown in the q-p' plane in Fig. 11, where q is the deviator stress and both q and p' are normalised for ν by means of the equivalent pressure p_e* on the INCL* (see Fig. 10). The data show that, according to Critical State Soil Mechanics, *dry* behaviour is recorded only for specimens swelled to overconsolidation ratios R (= p'_y/p') higher than 2, and that the q-p' states possible for the fissured clay are located inside the state boundary surface of the reconstituted clay, SBS*. Thus, the data confirm the framework of shear behaviour in Fig. 8b, i.e. the size of the SBS of the natural clay is smaller than that of the reconstituted, SBS*. The normalised stress paths of the fissured clay specimens consolidated beyond gross yield before shearing, confirm that the *wet* side of the SBS of the fissured clay (e.g., stress paths of specimens BENT-B and BENT-C in Fig. 11) increases in size with compression. Hence, a positive hardening component adds to volumetric hardening for the fissured mesofabric.

All these behavioural features are common to all the clays in Table 1 (Vitone and Cotecchia 2011; Cotecchia et al. 2014). It is not possible to report all the test data for a matter of space, therefore the BENT shear data are meant as representative of the behavioural trends exhibited by all the clays in the slopes of interest. These behavioural trends allow to infer that each of the slopes of reference is weaker than it would be if it was formed of clays of the same composition and consolidation state (i.e., having the same $\nu\text{-}\sigma'_{ij}$ at all points, x-y-z, as those in situ; Fig. 12), but reconstituted in the laboratory (Fig. 8). This is because for any clay element in the slope, of state $\nu\text{-}\sigma'_{ij}$ (Fig. 12a), fissuring causes a weakening with respect to the reconstituted clay, whatever the microstructure is like, as proven by the smaller size of the SBS of the fissured clay with respect to that of the reconstituted, SBS*, in the q-p'-ν space (Fig. 8b). The difference in size between the state boundary surfaces implies that, at any point in the slope (x-z: $\nu\text{-}\sigma'_{ij}$, Fig. 12a), the gross yield surface (yield surface in the figure) of the fissured clay is smaller than that of the reconstituted clay, as exemplified respectively by YS_F and YS* in Fig. 12b. Even stronger would be the slope if formed of the same clay, but unfissured and sensitive, due to a microstructure stronger than that of the reconstituted clay.

Table 2 reports the peak friction angles measured for the natural fissured clays in Table 1, ϕ'_{peak} (c'=0kPa is assumed), the post-peak friction angles, $\phi'_{post\text{-}peak}$, and the critical state friction angles of the reconstituted, ϕ^*_{cs}. These values were deduced from consolidated undrained shear tests in the triaxial (CIU). The data suggest that fissuring not only reduces the size of the SBS of the clay, but also the peak friction angles on the *dry* side (making them quite close to ϕ^*_{cs}), because it restrains the dilation rates of the overconsolidated clay. On the *wet* side, both the fissured clay and the reconstituted clay friction angles are rather low. Given the void ratios (see Table 1) and gross yield pressures in the slopes (Figs 9-10), the clays are overconsolidated in situ and exhibit a *dry* shear behaviour down to about 50-80 m, beyond which they tend to show a *wet* shear behaviour. It follows that the clay strength parameters vary in a limited range, despite their different origin, location and history, and provide the slopes with common weakness.

Table 2 also reports values of the residual friction angle, ϕ'_r, measured in the laboratory by means of either Bromhead ring shear tests or reversal direct shear tests. These values are representative of the very low strength of these high plasticity clays, in good agreement with those reported in the literature for clays of similar plasticity and composition (Lupini et al. 1981; Stark and Hussain 2013).

Fig. 13 shows the saturated permeability values, k_s, measured in oedometer tests on the fissured clays in Table 1 and on the same materials when reconstituted. The measurements have been carried with consolidation flow in the axial direction of the undisturbed sample. The k_s–e data refer to different stages of compression during the oedometer test (Terzaghi 1923).The ratios $\Delta e/\Delta \log k_s$, generally defined as C_k (Taylor 1948), decrease with compression for both natural and reconstitutes clays, similarly to what has been observed by Terzaghi et al. (1996).

Fig. 13 also shows the k_s associated to the in situ void ratio (deduced from the linear regression of the test data and indicated with circles). For the fissured samples, k_s results from the combination of both the very low permeability of the clay elements between the fissures and the high permeability of the fissures (Federico and Musso 1990). The figure shows that k_s of the fissured clay from laboratory testing is higher than 10^{-10} m/s and it is found to be higher (even of two orders of magnitude) than that of the same clay when reconstituted.

For fissures oriented and orthogonal to the flux direction (as for SCM scaly clay, F1/0°), k_s is lower than that measured for clays of random fissure orientation, (i.e., SEN scaly clay, F3), and further smaller (up to one order of magnitude) than for those having fissures oriented in the direction of the flux (F1/90°). The larger permeabilities resulting from fissuring predispose the slopes to larger rainfall infiltration. This makes possible an increase of the pore water pressures down to large depths, which is detrimental for the field operational strengths. These effects will be

shown to apply to the slopes here of reference. Hence, it may be envisaged that fissuring plays the role of internal factor predisposing the slope to failure not only for its effects on the clay mechanics, but also for its influence on the clay permeability.

LANDSLIDE MECHANISMS IN SLOPES FORMED OF FISSURED CLAY SEQUENCES

The Vadoncello landslide

Fig. 3 reports the map and the lithological section of the Vadoncello slope (Santaloia et al. 2001; Fig. 2c). In the section, the soils have been grouped into several soil complexes, according to a lithological screening and to the index properties of the clay samples (Table 1). Each complex represents a lithological sequence found recurrent in the slope.

In December 1993, a medium depth rotational slipping took place at the top of the slope and was followed downslope by an earth-flow (Hungr et al. 2014), characterised by both sliding along a shear band and full remoulding within the landslide body. The earthflow deposit, identified as complex G in Fig. 3b (about 10 m deep), includes remoulded scaly clays and rock debris. Landslide activity was monitored from 1994 until 1996 by means of both GPS and inclinometers; also piezometric monitoring was on at the same time.

As said before, SEN clays are characterised by friction angles that are particularly low both at peak and post-peak (Table 2). Furthermore, below 30-40 m depth they exhibit stress-strain states on the *wet* side (Santaloia et al. 2001), with corresponding friction angle, ϕ', lower than that of the dilative shallower clays. This condition, combined with the small size of the SBS of the SEN clays, allows for the occurrence at depth of large plastic straining due to even small changes in equilibrium (such as those effect of climate), and predisposes the slope to deep failure. Conversely, clay fissuring at depth does not give rise to relatively high permeability values (Fig. 13) and, hence, it does not predispose the slope to rainfall infiltration down to large depths. This has been confirmed by piezometers installed at larger depths. They have shown the presence of a deeper groundwater system, location of rather permanent piezometric heads; these are likely to be fed by the aquifer present in the karst limestone of the Picentini Mountains (Fig. 4) and are not significantly affected by rainfalls (Santaloia et al. 2001). Only the piezometric levels monitored in complex G have been found to be influenced by rainfall events in the short term (Santaloia et al. 2001).

In order to diagnose the failure mechanism and the triggering causes of the 1993 Vadoncello landslide, temporal geomorphological analyses have been carried out. It has been found that the 1993 event had been preceded, in 1980, by sliding in the lower part of the slope (Santaloia et al. 2001), subsidiary to the far larger and deeper Serra

dell'Acquara clay-slide, mobilised few hours after the 1980 Irpinia earthquake (V. Cotecchia et al. 1986). The Serra dell'Acquara landslide soils are named as complex I in Fig. 3b, at the toe of the Vadoncello slope, whereas the soils mobilised in the slope in 1980 represent complex H. Hence, the 1993 event was an evolution of a past instability. Furthermore, the analysis of the topographic monitoring data of 1995 (Fig. 14) shows that, while the highest displacement rates were taking place in the source area (area A in Fig. 14) and in the channel of the earth-flow (area B), the accumulation area (area C) was moving far more slowly, in a direction about parallel to the Serra dell'Acquara axis. GPS monitoring showed that this latter body was moving too, although very slowly, and I1 inclinometer monitoring (Fig. 3b), at the toe of the slope (area C, Fig. 14), gave evidence to the occurrence of sliding at 15 m depth within the Serra dell'Acquara clay slide. Therefore, the landslide reactivated in 1993 was the combination of a relatively fast shallow landslide process and a deeper, far slower deformation process, resulting from the interaction of the Vadoncello slope with the very slowly active Serra dell'Acquara clay-slide (Figs 3 and 14). The moving slope toe may be then recognized as the trigger of variations with time of the slope geometry. Given the available soil strengths, this brought the slope to instability in 1993, with rotational slipping at the top and earthflowing down-slope (Santaloia et al. 2001).

Numerical modelling was carried out by means of the finite difference code FLAC 2D (Itasca Consulting Group 2000), implementing the geotechnical model shown in Fig. 15, extended upslope of about 500 m (Santoro 1999; Cotecchia et al. 2000). Based on laboratory test results (Tables 1 and 2, Figs 8, 9 and 13), the geotechnical model includes the different soil complexes, all modelled using a linear elasto-plastic non associated Mohr-Coulomb model, with strain softening post-peak. Dilative and contractive zones (of *dry* and *wet* behaviour, respectively) were distinguished within each complex (Cotecchia et al. 2000), the *wet* portions being characterised by $c'=0$ kPa and $\phi'=\phi'_{cs}$ yield parameters, whereas for the dilative portions, c' and ϕ' values shown in Fig. 15 were used. Yield was assumed to be reached at about 10% shear strain and followed by strain softening, to a yield locus characterised by $c'=0$ kPa and $\varphi'_r=5.5°$ (reached at 50% shear strain). Both the shallow and the deep groundwater systems were modelled, considering the piezometric levels compatible with the two water tables in Fig. 15. A very slow-moving boundary at the slope toe was also implemented in the numerical model, in order to simulate the Serra dell'Acquara landsliding. The numerical results, in terms of displacement values, are synthesized in Fig. 16. Each boundary within areas 1, 2 and 3 is characterised by quasi-uniform displacements (average values in the figure). These represent the results of three numerical analyses: A) no seepage and pure submersion of the soils below the two different water

tables, B) seepage complying with the different water tables in the deep and shallow seepage domains, but no toe translation, and C) both seepage and toe translation. The numerical results confirm that the internal slope factors and the toe boundary condition combine to generate a complex landslide mechanism: a rather fast rotational slipping upslope (area 1 in Fig. 16) and a shallow earthflow downslope. In particular, the earthflow is predicted to reach inclinometer I1 only when the moving toe boundary is modelled. Furthermore, numerical modelling confirms the occurrence of lower rate movements at larger depths.

The SEN case study exemplifies how, in the Apennines, often shallow fast landslides may be just the local outcropping of far larger and deeper systems at marginal stability.

The Pisciolo landslide basin

Fig. 5 reports the geological setting of the PI hillslope (Fig. 2c), location of clayey turbidites of the Paola Doce Formation (PD 1 and PD2 clays in Table 1). Due to the presence of an anticline, that caused uplifting of the central portion of the hillslope, Red Flysch outcrops in the centre of the landslide basin (Fig. 5). Also, a normal fault crosses the hillslope with an East-West trend and separates northern and southern sectors. In the past, this fault was location of a deep gorge, hosting the Pisciolo stream (Fig. 5), whose section size progressively decreased in the last 50 years.

Clay fraction and plasticity index decrease moving from the lower PD1 clays to the upper PD2 (Table 1). The compression behaviour, strength parameters and permeability values of these clays are shown in Fig. 9, Table 2 and Fig. 13 respectively.

Ten clay-slides are located within the PI hillslope (Fig. 5). They are moving at rates from few millimetres to tens of centimetres per year (Cotecchia et al. 2014), causing damage to both the Apulian Aqueduct pipeline and the road located at the base of the slope. The most severe damage has been observed in the southern portion of the hillslope, where landslides C9, C and A are located (Fig. 5). These landslide bodies, involving both PD and RF clays, have a common toe about the road, intercepted by inclinometer I12 (Fig. 17). Inclinometer I5, installed in the central part of body A, gives also evidence to the retrogression of movements upslope, down to large depths, although so far it has not been sharply bent at any depth. In Fig. 17 the inclinometer data intercepting the shear bands of bodies L and G are also reported (Fig. 5). Based on the data, the landslides at PI can be classified as multiple retrogressive landslides, of medium to large depth (Fig. 5b).

The piezometric levels have been found to reach few metres below ground level in several piezometers (Fig. 5)

installed from small to large depths (i.e., 60 m). As discussed earlier, the laboratory measurements showed that the saturated permeability of the PD clays can be even higher than 10^{-10} m/s at the element scale (Fig. 13). Moreover, k_s higher than 10^{-9} m/s has been measured in situ, through constant head permeability tests (Pedone 2014). Such a relatively high permeability of the clay matrix, together with the higher permeability of the rock strata, ease the rainfall infiltration and the occurrence of high piezometric heads and low shear strengths down to large depths.

Limit equilibrium back-analyses (Morgenstern and Price 1965), implementing the measured piezometric heads, have been performed to evaluate the operational friction angles. These have been found to be either close to the peak friction angles, e.g. bodies A, C, G and L, or to the post-peak ones, e.g. bodies F and C9 (see Table 2). Therefore, landslide bodies A, C, G and L represent first-time failure processes, whereas bodies F and C9 represent an evolution of past failures, in agreement with the temporal analysis of aerial photos. In 1955 (Fig. 18), only bodies F and C9 were present, although smaller than today; only soil slips occurred in the southern slope sector. At that time, the Pisciolo stream flew in a deep gorge, representing the main discharge path of the water run off on the slope. Subsequent aerial photos show that, in the last 60 years, progressive widening and deepening of landsliding have taken place. At the same time, the section of the Pisciolo stream has decreased, with a consequent loss of discharge capacity. It is envisaged that this has promoted rainwater ponding, infiltration and increase of the piezometric levels, bringing about the widening and deepening of landsliding.

As shown in Fig. 19, with particular reference to the toe of bodies C9, C and A, a seasonal variation characterises the current landslide displacement rates, both at depth (inclinometer I12) and at ground surface (GPS sensor S2), with maximum values at the end of winter and minimum values at the end of summer. Also the piezometric heads measured in the same area (cells at 15 and 36 m depth along P7) and the 180-day cumulated rainfall (recorded at the Melfi weather station) follow a similar fluctuation trend. Hence, the pluviometric regime of the area and the clay hydraulic properties appear to allow for seasonal variations of the pore pressures. These may trigger accelerations of the fully developed landslide bodies, such as those measured at the toe of the slope in the southern sector (bodies C9 and C; Fig. 5). Piezometric data similar to those shown in Fig. 19 have been collected all over the hillslope.

The transient seepage in the slope, influenced by the slope-atmosphere interaction, has been modelled by means of finite element analyses of a two-dimensional slope model, implementing the hydraulic permeabilities and the water retention properties measured both in situ and in the laboratory (Cotecchia et al. 2014; Pedone 2014). In particular, the FEM code Seep/w (GeoSlope International Ltd. 2004), that integrates the Richards' equation (1931), has been used to

model the slope section II in Fig. 5b. The mesh of the model shown in Fig. 20 is formed of quadrilateral elements. The saturated permeability of both PD1 and PD2 clays has been set as $k_s=1*10^{-9}$ m/s, according to the above mentioned in situ measurements. Only for the top layers that happen to be above the water table during part of the year, the model accounts for the water retention curve measured in the laboratory on samples taken by 2 m depth (Cotecchia et al. 2014). Retention data have been fitted using the van Genuchten (1980) equation, while the hydraulic conductivity model proposed by the same author has been employed to simulate the variation of the permeability coefficient with suction. Furthermore, an organic top soil layer has been implemented, whose saturated permeability is $k_s=1*10^{-8}$ m/s. Pore pressures constantly equal to zero have been imposed at the very top and at the bottom of the slope, according to the presence of a spring and of the Ofanto River respectively. The lowest boundary of the model has been assumed as impermeable, whereas the net rainfalls referred to the period September 2006-August 2007 have been cyclically applied at the top of the mesh. Net rainfalls result from the difference between total rainfalls and evapo-transpiration fluxes, the latter evaluated by means of the FAO Penman-Monteith method (Allen et al. 1998).

The numerical results have been compared with the piezometric data logged down the verticals P7 and P5 (Figs 5b and 20) for modelling validation (Fig. 21). The variations in piezometric head predicted by the numerical model (continuous lines in Fig. 21) are close to those measured (squares in Fig. 21) down borehole P7, especially once the fractured rock inclusions are also implemented in the analyses ($k_s = 10^{-6}$ m/s). On the contrary, the predicted fluctuations are much smaller than those recorded along the vertical P5 (Fig. 21). This vertical is very close to the sandy deposit N (Fig. 5a) and this is probably causing three-dimensional effects not accounted for in the 2D numerical modelling.

The Pisciolo case study is representative for landsliding influenced by the slope-atmosphere interaction recurrent in the Southern Apennines. In particular, at Pisciolo, this interaction is a triggering cause that combines with the internal predisposing factors cited before.

The Santa Croce di Magliano landslides

As depicted in Fig. 6, the slopes at SCM are formed by turbidites part of the Daunia Unit (Fig. 2c) and are diffusely location of failure processes. These start in the scaly clay strata (SCM scaly clay soils), whose mesofabric and geotechnical properties have been discussed above (Figs 9-11 and 13, Tables 1 and 2). Thereafter they involve the BENT clays and the FAE rock slab (Fig. 6) located upslope. Most of the sliding surfaces have toe about the river

flowing at the bottom of the valleys, either North or South of the village (Fig. 6). Several springs occur about the rock-clay contact, which represent the outcropping of a seepage domain whose water table occurs at 2-3 m depth below the slope ground surface.

The SCM scaly clays, along with the BENT clays, are of even higher plasticity than the SEN and PI clays (Fig. 2; Table 1). Due to these intrinsically weak clays, fissuring provides a further source of strength reduction. Moreover, in this case, the clay strength does not benefit from the presence of as many coarse strata and floating rock beddings as for the SEN and the PI slopes. Within the simpler SCM sequences (Fig. 6b), the landslide mechanisms are mainly roto-translational sliding, as shown by the inclinometer data in Fig. 6c. This intercepted a sliding surface at 22 m depth, along which the displacement rates were about 14 mm/month during a period of high landslide activity (Fig. 6c).

The failure mechanism recognized in the southern slope location of the inclinometer may be considered representative for most of the sliding phenomena at SCM (Cotecchia et al. 2007; Fig. 6a). The only difference between the northern and the southern slopes of SCM promontory is that, where in the northern slopes landsliding has been on for a longer period, reaching and involving the top FAE rock slab (Fig. 6), in the southern slopes, it is more recent and caused more limited variations of the original morphologies. The back-analyses of the northern landslides result in mobilised friction angles ϕ'_m=17°–18° (c'=0 kPa), which are far above the residual friction angle of the clays (Table 2) and only a bit lower than the clay peak friction angles on the *dry* side (Cotecchia et al. 2003, 2007). Conversely, the mobilised friction angles for the southern landslides are smaller, ϕ'_m=12°-13°. The high operational strengths in the northern slopes may appear in contrast with the more mature activity of landsliding in such slopes. However, it should be considered that the long-term landsliding in these slopes has caused remoulding of the scaly clays that brings about an increase in the shear strength of the clays, as shown by the framework in Fig. 8b. This remoulding has not taken place yet in the southern slopes of the promontory, which, therefore, are weaker than at North.

CONCLUSIONS

The three case studies have given evidence to the failure processes that may take place and bring about landsliding in slopes formed of tectonized turbidites. The landslide mechanism may be either simple non-circular sliding (SCM), or multiple retrogressive clay sliding (PI), or a combination of deep sliding with shallow earth-flowing (SEN) but, in general, it is of medium depth to deep and slow to extremely slow.

The tectonized soil sequences belong to different geological formations, but share major similarities in the hydro-mechanical behaviour of the clays, which are the weakest lithotype within the slopes and control the failure progression. These mechanical properties have been shown to fit a framework where the fissured clay strength is not only lower than that of the unfissured structured clay, but also than that of the unfissured reconstituted clay. This finding has allowed to recognise, as first, that slopes in fissured clays are weaker than slopes in reconstituted clays; as second, that the mechanical properties of the high plasticity fissured clays are an internal predisposing factor of landsliding.

The clay fissuring and the fractured rock interbeddings have also been recognized as sources of larger field permeabilities, which predispose the slopes to infiltration rates down to large depths higher than those expected for clays. This hydraulic feature allows for large piezometric heads at depth and relatively smaller available strengths. Failure has been found to start generally in the fissured clays and to propagate depending on the slope stratigraphic features. These, along with both the mechanical and hydraulic boundary conditions of the slope system, control the type of landslide mechanism. For example, simple sliding is more likely to occur in slopes of simpler stratigraphy and characterised by standard boundary conditions, such as the SCM slopes. Here, three main soil strata, slightly dipping downslope, occur from bottom to top. More complex sliding, or otherwise earth-flowing, is more likely to occur in slopes of more complex stratigraphy, where the soil sequences are more chaotic, as at PI and SEN. Furthermore, earth-flowing at SEN has been recognized to be only the shallow process within a wider and deeper failure mechanism, which relates to a moving boundary at the slope toe. Such landslide features have been verified by numerical modelling and also found to apply at other sites in the southern Apennines, e.g. Toppo landslide (Cotecchia et al. 2009).

Finally, it has been shown that slide accelerations recorded at the end of winter–early spring may be due to the reach of maximum pore water pressures as effect of cumulated seasonal rainfall infiltration. The seasonal piezometric excursions have been measured and, thereafter, predicted through a rather accurate modelling of the transient seepage in the slope, accounting for the hydraulic soil properties, both when saturated and in partial saturation conditions.

Acknowledgments
The authors wish to thank the Apulian Aqueduct SPA (2008-2011), the Apulia Region (PS_119- 2006-2010), the Italian Ministry for Research and University (PRIN 2001, 2007, 2010-2011) and European Community-Environment Programme (1994-1996) for providing the financial support that has permitted the studies discussed in the paper.

REFERENCES

AGI (1979) Some Italian experiences on the mechanical characterisation of structurally complex clay soils. In International Society of Rock Mechanics (ed.), Int Soc Rock Mech 4th Int Cong 1, pp 827-846

Airò Farulla C, Ferrari A, Romero E (2010) Volume change behaviour of a compacted scaly clay during cyclic suction changes. Canadian Geotechnical Journal 47(6):688-703

Allen RG, Pereira LS, Raes D, Smith M (1998) Crop evapo-transpiration, guidelines for computing crop water requirements. FAO irrigation and drainage paper 56

ASTM (1985) Classification of Soils for Engineering Purposes: Annual Book of ASTM Standards, D 2487-83, 04.08, American Society for Testing and Materials, pp 395–408

BSI British Standards (1986) Code of practice for foundations. BSI BS8004

Burland JB (1990) On the compressibility and the shear strength of natural clays. Géotechnique 40(3):329-378

Calabresi G, Manfredini G (1973) Shear strength characteristics of the jointed clay of S. Barbara. Géotechnique 23(2):233-244

Cicolella A, Picarelli L (1990) Decadimento meccanico di una tipica argilla a scaglie di elevata plasticità. Italian Geotechnical Journal 24:5-23

Cotecchia F, Chandler RJ (2000) A general framework for the mechanical behaviour of clays. Géotechnique 50(4):431-447

Cotecchia F, Santaloia F (2003) Compression behaviour of structurally complex marine clays. Soft Ground Engineering in Coastal Areas; Proc Nakase Memorial Symp, Yokosuka Japan, pp 63-72

Cotecchia F, Vitone C (2011) On the model requirements to predict the behaviour of fissured clays. XV ECSMGE, Athens, Greece, pp 525-530

Cotecchia F, Santaloia F, Santoro F (2000) Movements in a tectonized soil slope: comparison of monitoring data and modelling results. Int Conf Geotechnical & Geological Engineering, Melbourne, Australia

Cotecchia F, Cafaro F, Melidoro G, Mitaritonna G (2003) Mechanical behaviour of natural tectonized bentonites. Proc Int Workshop Geotechnics of Soft Soils, Amsterdam, pp 397-402

Cotecchia F, Vitone C, Cafaro F, Santaloia F (2007) The mechanical behaviour of intensely fissured high plasticity clays from Daunia. Proc 2nd Int Workshop Characterisation and Engineering Properties on Natural Soils, Singapore, Taylor & Francis London, pp 1975-2003

Cotecchia F, Mitaritonna G, Elia G, Santaloia F, Lollino P (2009) Meccanismi di frane in pendi in argille dell'Italia Meridionale ed effetti delle precipitazioni meteoriche. 1st Int Workshop on Landslides: rainfall induced landslide and nowcasting models for early warning system, pp 31-43

Cotecchia F, Santaloia F, Vitone C, Palladino G (2012) A slow and complex landslide process in the Southern Apennines (Italy). Proceedings 11th Int Symp Landslides and 2nd North American Symp Landslides. Banff, Alberta, Canada, in Landslides and Engineered Slopes: Protecting Society through Improved Understanding, Taylor & Francis Group 1, pp 1009-1016

Cotecchia F, Pedone G, Bottiglieri O, Santaloia F, Vitone C (2014) Slope – atmosphere interaction in a tectonized clayey slope: a case study. Italian Geotechnical Journal 1:34-61

Cotecchia V (1986) Ground displacement and slope instability triggered off by the earthquake of November 23, 1980 in Campania and Basilicata. Int Symp Engineering geology problems in seismic areas, Geol App Idr 21:31-100

Croce A (1971) Opening address of the International Symposium on 'The Geotechnics of structurally complex formations'. Capri 2, pp 148-151

Cruden DM, Varnes DJ (1996) Landslides types and processes. In: Turner AK, Schuster RL (eds) Landslides: investigation and mitigation, Transp Research Board Special Report 247. National Academy Press, WA, pp 36–75

Dewey JF, Helman ML, Turco E, Hutton DHW and Knott SD (1989) Kinematics of the Western Mediterranean. In MPD Coward, D Park, RG (Editor), Alpine Tectonics. Geological Society, pp 265-283

Di Nocera S, Matano F, Pescatore T, Pinto F, Quarantiello R, Senatore M R, Torre M (2006) Schema geologico del transetto Monti Picentini orientali - Monti della Daunia meridionali: unità stratigrafiche ed evoluzione tettonica del settore esterno dell'Appennino meridionale. Boll Soc Geol It 125:1-20

Desrues J, Viggiani G (2004) Strain localization in sand: an overview of the experimental results obtained in Grenoble using stereophotogrammetry. Int J Numer Anal Meth Geomech28:279-321

Doglioni C (1991) A proposal of kinematic modelling for W-dipping subduction – Possible applications to the Tyrrhenian Apennines system. Terra Nova 3:423–434

EC Project Report (1996) Landslide evolution controlled by climatic factors in a seismic area. Prediction methods and warning criteria. Final Technical Report

Fearon R, Coop M R (2000) Reconstitution - what makes an appropriate reference material? Géotechnique 50(4):471-477

Fearon R, Coop MR (2002) The influence of landsliding on the behaviour of a structurally complex clay, Quarterly Journal of Engineering Geology and Hydrogeology 35:25-32
Federico F, Musso A (1990) Consolidazione monodimensionale di argille a scaglie. Gruppo Nazionale di coordinamento per gli studi di Ingegneria Geotecnica, Roma, pp127-130
Fenelli, GB, Paparo Filomarino M, Picarelli L, Rippa F (1982) Proprietà fisiche e meccaniche di argille varicolori dell'Irpinia. Rivista Italiana di Geotecnica 3:110-124
Fookes PG, Denness B (1969) Observational studies on fissure patterns in cretaceous sediments of South-East England. Géotechnique 19(4):453-477
Gasparre A, Nishimura S, Coop MR, Jardine RJ (2007) The influence of structure on the behaviour of London Clay. Géotechnique 57(1):19–31
GEO-SLOPE International Ltd (2004) Seepage modeling with SEEP/W, user's guide. Calgary, Alberta, Canada
Hight DW, Gasparre A, Nishimura S, Minh NA, Jardine RJ, Coop MR (2007) Characteristics of the London Clay from the Terminal 5 site at Heathrow Airport. Géotechnique 57(1):3-18
Hungr O., Leroueil S., Picarelli L. (2014) The Varnes classification of landslide types, an update. Landslides 11: 167-194.
ISRM (1993) Metodologie per la descrizione quantitativa delle discontinuità nelle masse rocciose. Italian Geotechnical Journal 2:151-197
Itasca Consulting Group (2000) FLAC2D Version 4.0. Minneapolis: Itasca Consulting Group
Leroueil S, Vaughan P (1990) The general and congruent effect of structure in natural soils and weak rocks. Géotechnique 40(3):467-488
Lo KY (1970) The operational strength of fissured clays. Géotechnique 20(1):57-74
Lupini JF, Skinner AE and Vaughan PR (1981) The drained residual strength of cohesive soils. Géotechnique 31(2):181-213
Malinverno A, Ryan WBF (1986) Extension in the Tyrrhenian Sea and shortening in the Apennines as result of arc migration driven by sinking of the lithosphere. Tectonics 5:227–245
Marsland A (1971) The shear strength of stiff fissured clays. Roscoe Memorial Symp, Cambridge Univ, pp 59-68
Melidoro A, Melidoro G, Panaro V (2002) Deformazioni gravitative dei versanti nei terreni fliscioidi con argille a bentoniti di Santa Croce di Magliano (Molise). Quarry & Construction:11-17
Morgenstern NR, Price VE (1965) The analysis of the stability of general slip surface. Géotechnique 15(1):79-93
Morgenstern NR, Eigenbrod KD (1974) Classification of argillaceous soils and rocks. Jour Geotech Eng Div, ASCE 100(10):1137-1156
Ogniben L (1969) Schema introduttivo alla geologia del confine calabro-lucano. Mem Soc Geol Ital, 8:453-763
Parotto M, Praturlon A (2004) The Southern Apennine Arc. In U. Crescenti, S. D'Offizi, S. Merlino & L. Sacchi (eds), Geoogy of Italy, Special Volume of Italian Geological Society for the International Geological Congress 32:33-58
Patacca E, Scandone P (2007) Geological interpretation of the CROP-04 seismic line (Southern Apennines, Italy). In: Mazzotti A, Patacca E, Scandone P(Eds), Results of the CROP Project, Sub-project CROP-04 So 7, pp 297-315
Pellegrino A, Picarelli L (1982) Contributo alla caratterizzazione geotecnica di formazioni argillose intensamente tettonizzate. Geologia Applicata ed Idrogeologia 20(2):155-192
Pedone G (2014) Interpretation of slow and deep landslides triggered by slope-atmosphere interaction in slopes formed of fissured clayey turbidites. PhD thesis, Technical University of Bari, Italy
Pescatore T, Senatore MR (1986) A comparison between a present-day (Taranto Gulf) and a Miocene (Irpinian Basin) foredeep of the Southern Apennines (Italy). Spec Publs Int Ass Sediment 8:169-182
Pescatore T, Renda P, Schiattarella M, Tramutoli M (1999). Stratigraphic and structural relationships between Meso-Cenozoic Lagonegro basin and coeval carbonate platforms in southern Apennines, Italy. Tectonophysics315:269-286
Pescatore T, Di Nocera S, Matano F, Pinto F (2000) L'Unità del Fortore nel quadro della geologia orientale dei Monti del Sannio (Appennino Meridionale). Boll Soc Geol It 119:587–601
Petley DJ (1984) Shear Strength of Over-Consolidated Fissured Clay. Landslides; Proc Int Symp 2, pp 167-172
Picarelli L, Olivares L (2004) Mechanical behaviour of highly sheared clay shales. Advances in Geotechnical Engineering: The Skempton Conference - Advances in Geotechnical Engineering, ICEl, pp 580-591
Richards LA (1931) Capillary conduction of liquids through porous media.Physics 1:318-333
Santaloia F, Cotecchia F, Polemio M (2001) Mechanics of a tectonized soil slope: influence of boundary conditions and rainfalls. Quart Journ of Eng Geol 34:165-185
Santoro F (1999) Meccanismi di deformazione di pendii in formazioni strutturalmente complesse. Il caso della frana Serra dell'Acquara – Vadoncello (Senerchia – AV). PhD thesis, Technical University of Bari, Italy
Scrocca D, Carminati E, Doglioni C (2005) Deep structure of the southern Apennines, Italy: Thin-skinned or thick-

skinned? Tectonics 24:1–20.
Schofield AN, Wroth CP (1968) Critical state soil mechanics. London: McGraw-Hill
Sella N, Dorci C, Riva A (1988) Sintesi geopetrolifera della Fossa Bradanica (avanfossa della catena appenninica meridionale). Mem Soc Geol It 41:87–107
Silvestri F, Vitone C, d'Onofrio A, Cotecchia F, Puglia R, Santucci de Magistris F (2007) The influence of meso-structure on the mechanical behaviour of a marly clay from low to high strains. Geotechnical Tatsuoka Symposium, Rome, Hoe I Ling et al eds, Soil Stress-Strain Behaviour: Measurement, Modelling, Analysis, Springer, the Netherlands, pp 333-350
Stark T, Hussain M (2013) Empirical Correlations: Drained Shear Strength for Slope Stability Analyses. J Geotech Geoenviron Eng, 139(6): 853–862
Taylor DW (1948) Fundamentals of soil mechanics. John Wiley & Sons, New York
Terzaghi K (1923) Die Berechnung der DurchlaÈssigkeitsziffer des Tones aus dem Verlauf der hydrodynamischen Spannungserscheinungen. Sitzungber. Akad Wiss Wien 132, pp 125-138
Terzaghi K (1936) Stability of slopes in natural clays. Proc. 1st Conf. On Soil Mechanics, Harvard, 1: 161-185
Terzaghi K (1950) Mechanisms of landslides. Geological Society of America, Berkley, pp 83-123
Terzaghi K, Peck RB, Mesri G (1996) Soil mechanics in engineering practice. John Wiley & Sons, New York
van Genuchten MT (1980) A closed form equation for predicting the hydraulic conductivity of unsaturated soils. Soil Science Society of America Journal, 44:892-898
Vitone C (2005) Comportamento meccanico delle argille da intensamente a mediamente fessurate. PhD thesis, Technical University of Bari, Italy
Vitone C, Cotecchia F (2011) The influence of intense fissuring on the mechanical behaviour of clays. Geotéchnique 61(12):1003-1018
Vitone C, Cotecchia F, Desrues J, Viggiani G (2009) An approach to the interpretation of the mechanical behaviour of intensely fissured clays, Soils & Foundation Journal 49(3):355-368
Vitone C, Cotecchia F, Viggiani G (2012) Localisation processes and size effects for fissured clay specimens. Advanced Multiphysical Testing of Soils and Shales (AMTSS) Workshop In Springer Series in Geomechanics and Geoengineering, Laloui Ferrari Eds, pp 219-225
Vitone C, Cotecchia F, Viggiani G, Hall SA (2013a) Strain fields and mechanical response of a highly fissured bentonite clay, Int J Numer Anal Meth Geomech 37:1510-1534
Vitone C, Viggiani G, Cotecchia F, Hall SA (2013b) Localized deformation in intensely fissured clays studied by 2D digital image correlation, Acta Geotechnica 8:247-263
Walker BF, Blong RJ, McGregor JP (1987) Landslide classification, geomorphology and site investigation. Soil Slope Instability and Stabilisation The Netherlands: Balkema, pp 1-5

Figure
Click here to download Figure: Figures_Cotecchia et al_2nd_Revision.docx

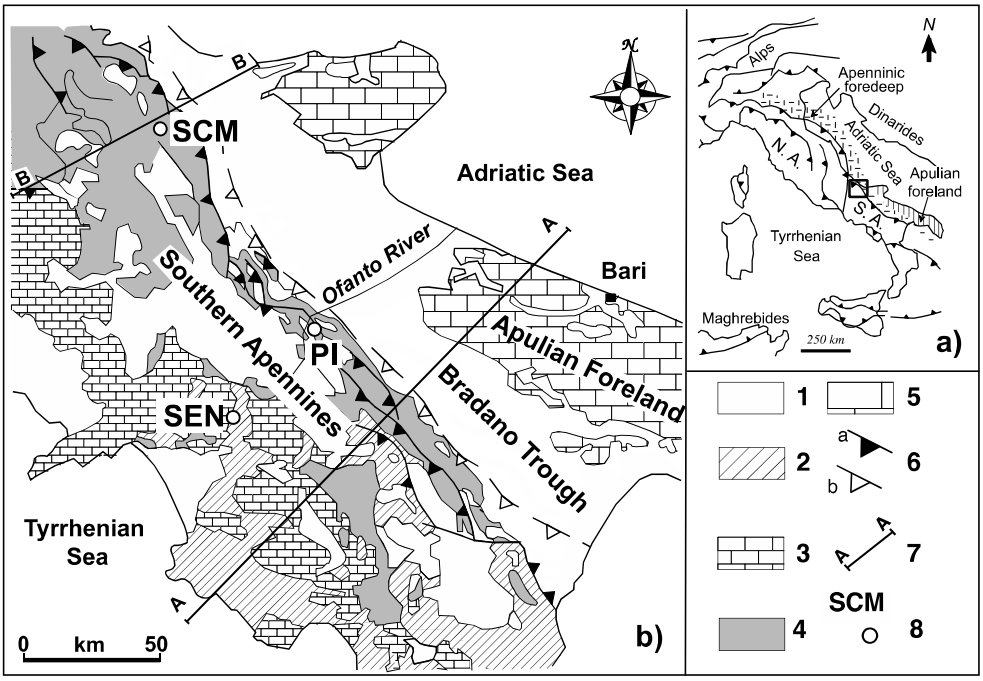


Fig. 1 (a) Schematic structural map of Italy (N.A. - Northern Apennines, S.A. - Southern Apennines) and (b) simplified geological map of the Southern Apennines (modified from Scrocca et al. 2005). Key: (1) marine to continental deposits, thrust-sheet-top deposits (Late Pliocene-Holocene); (2) Liguride-Sicilide Units and related ancient thrust-sheet-top deposits; (3) Apennine Platform Units and related silicoclastic foredeep deposits; (4) Lagonegro-Molise Units and related silicoclastic foredeep deposits; (5) Apulian Platform Units; (6) main thrusts (a) and buried Apenninic thrust front (b); (7) cross-section lines shown in Fig 2c; (8) slopes discussed in the paper (SEN-Vadoncello slope; PI-Pisciolo hillslope; SCM – Santa Croce di Magliano slopes).

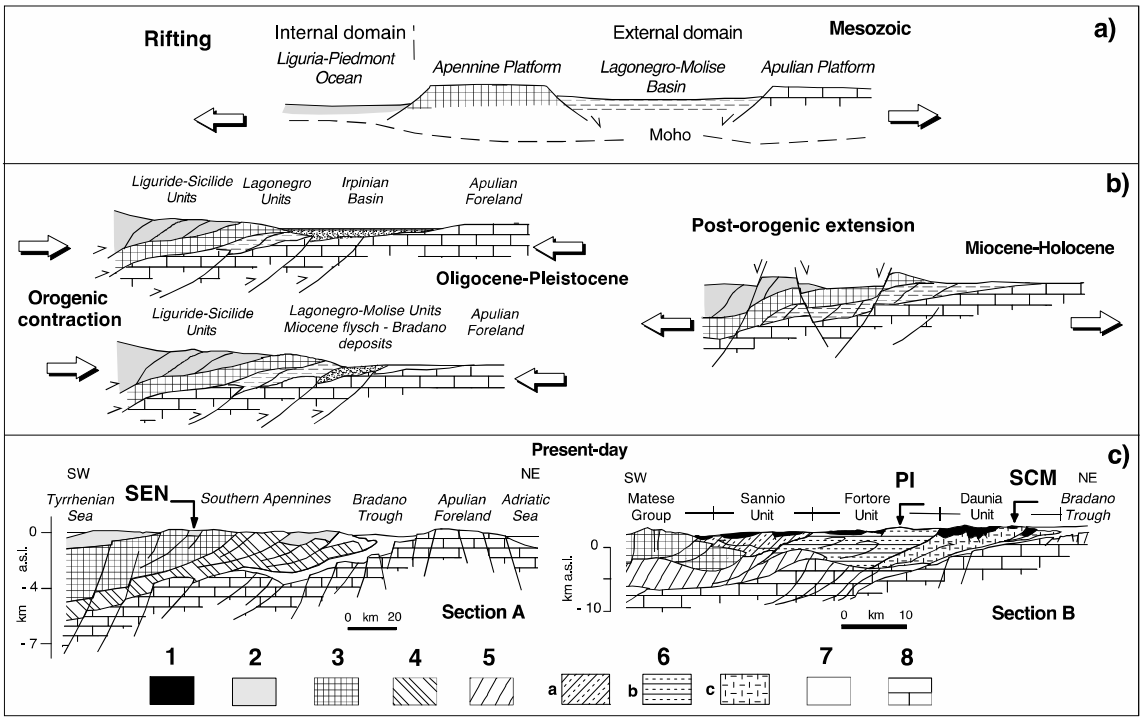


Fig. 2 Paleogeographic domains of the Southern Apennines during the Mesozoic Era (a), geological sketches (b) showing the main tectonic events responsible for the emplacement of the Southern Apennines (not to scale; after Parotto and Praturlon 2004, modified); c) schematic geological cross sections through both the southern Apennines thrust belt-foredeep-foreland system (Section A; after Sella et al. 1988, modified) and the north-eastern edge of the Sannio-Daunia Apennines (Section B; after Pescatore et al. 2000) - location of the sections in Fig. 1. Key: (1) plio-miocenic silicoclastic units; (2) Liguride-Sicilide Units (SEN soils); (3) Apennine Platform Units; (4) undifferentiated Lagonegrese-Molise Units; (5) lower sequences of the Lagonegrese-Molise Units; (6) upper sequences of the Lagonegrese-Molise Units (a: Sannio Unit, b: Fortore Unit – PI soils, c: Daunia Unit – SCM soils); (7) Bradano Trough Unit; (8) Apulian Platform Units.

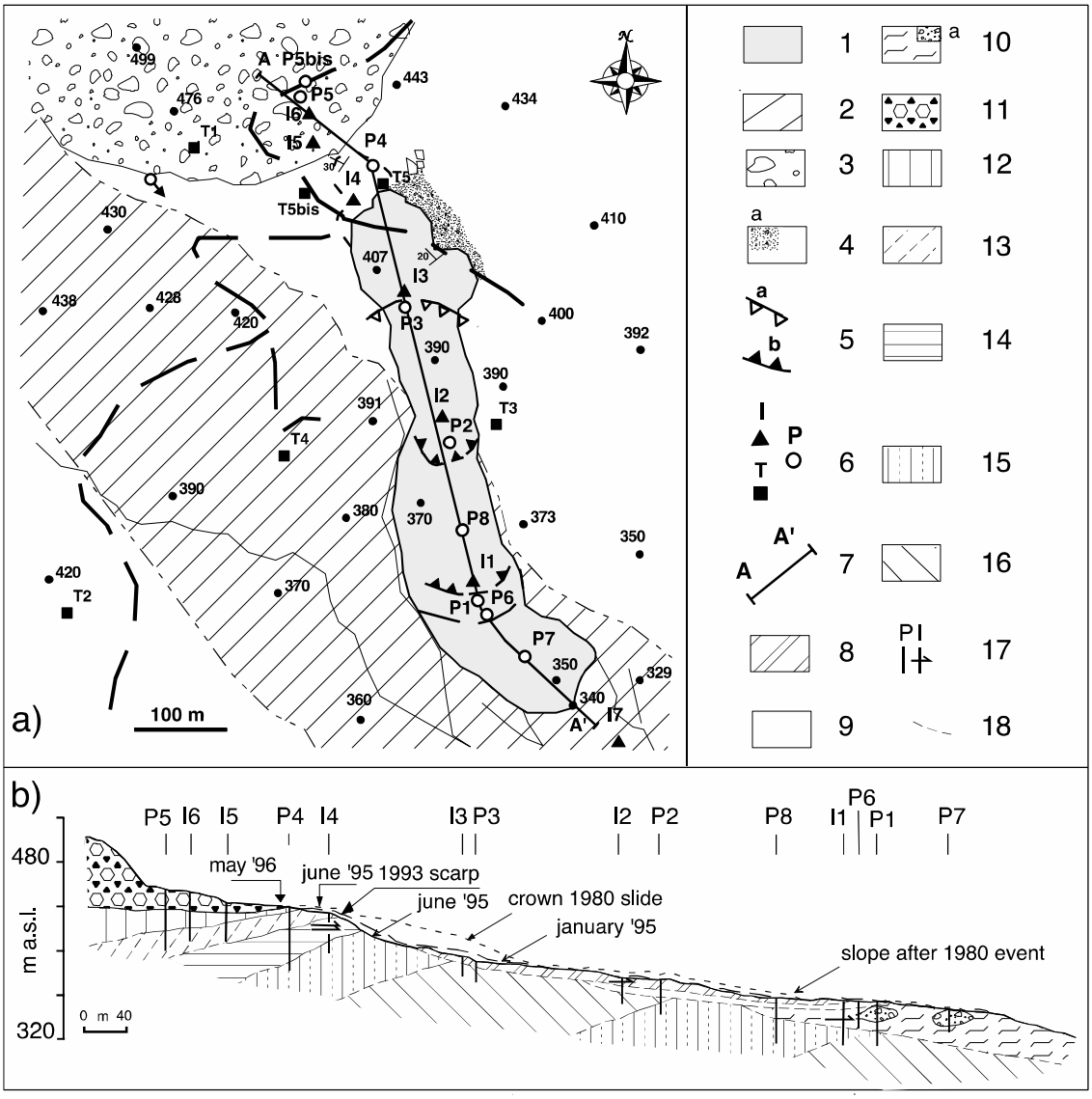


Fig. 3 Geological map (a) and section A-A' (b) of the Vadoncello slope (after EEC project 1996, Santaloia et al. 2001, modified); Keys: 1) 1993-'95 Vadoncello landslide; 2) Serra dell'Acquara landslide; 3) debris slab; 4) Variegated Clay Formation (SEN soils) with calcareous detritus (a); 5) 1980 crown (a), internal toes (b); 6) P-piezometers, I-inclinometers and T-topographic control stations (after EEC Report 1996; modified); 7) line of the section A-A'; Soil Complexes: 8) G, 9) H, 10) I with calcareous blocks floating in it (a), 11) A, 12) B, 13) C, 14) D, 15) E, 16) F; 17) piezometers (P1-P8) and inclinometers (I1-I7) with depth of shearing; 18) sliding surface.

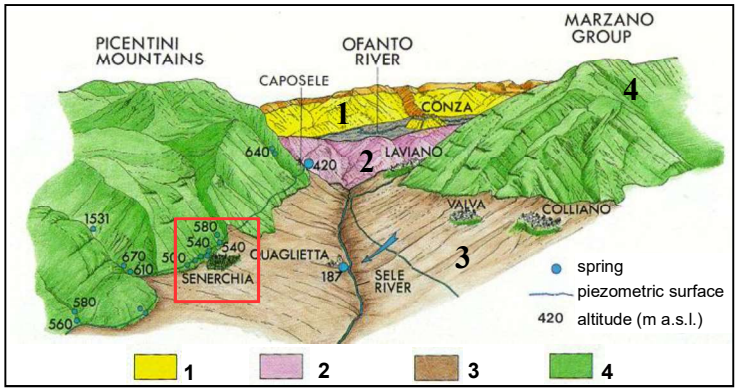


Fig. 4 Schematic view of the high Sele River Valley, location of the Senerchia slopes (after Cotecchia V. 1986, modified); Key: (1) Pliocene deposits; (2) Neogene and Sicilide Units; (3) Sicilide Unit (Lower Miocene-Cretaceous); (4) Apennine Carbonate Platform Units (Eocene-Upper Triassic).

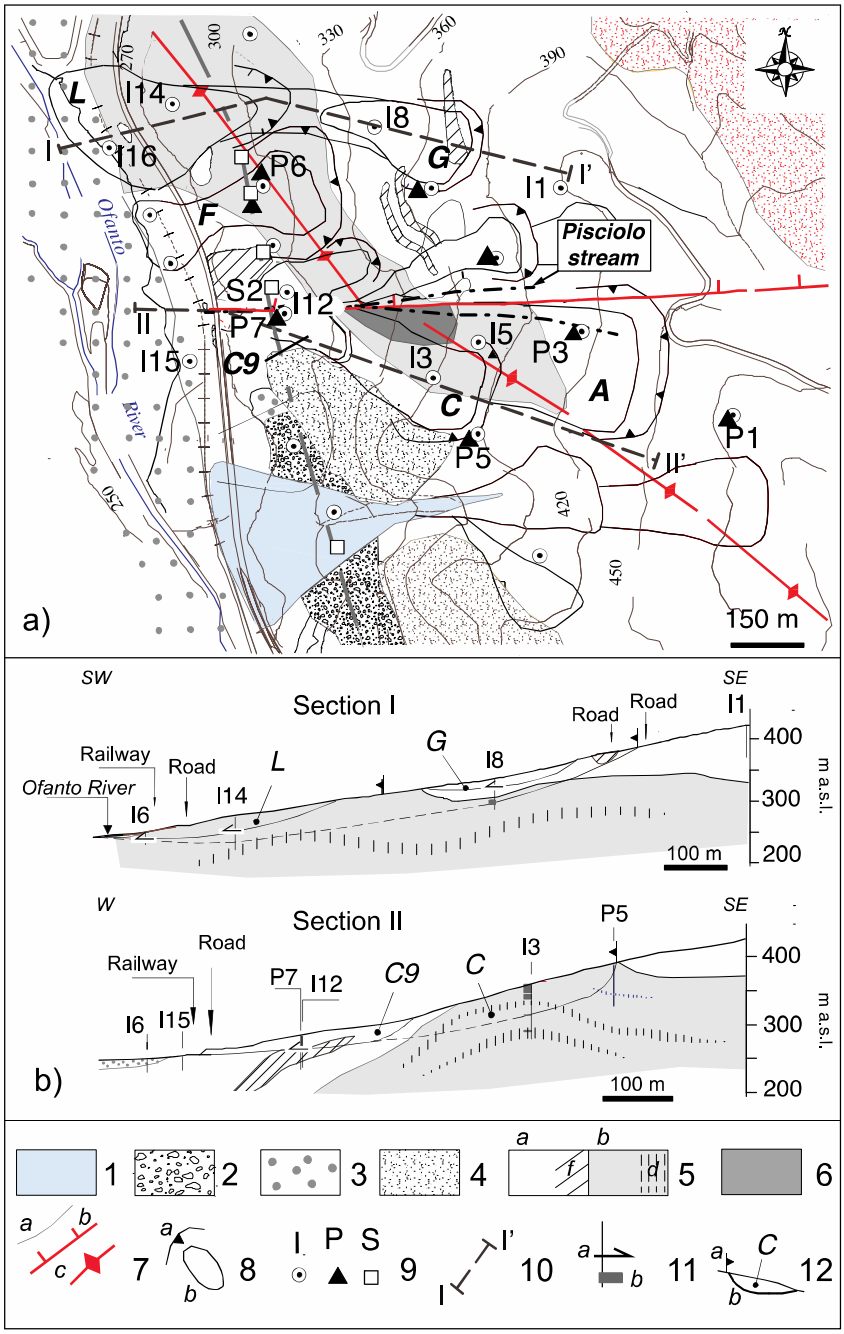


Fig. 5 Geological map (a) and sections (b) of Pisciolo hillslope. Key: 1) fan deposit; 2) debris deposit; 3) alluvial deposit; 4) N; 5) PD2 (a) PD1 (b), f-locally fractured rocky strata, d-disarranged rocky strata; 6) R with rock or coarse-grained intervals; 7) stratigraphic contact (a), fault (b), anticline axis (c); 8) landslide: crown (a), body (b); 9) boreholes equipped with piezometers (P) or inclinometers (I), GPS sensor (S) – only the labels of the boreholes mentioned in this paper are reported; 10) line of the section shown in the frame b) of the figure; 11) boreholes: inclinometer shear bending (a), remoulded soil portions (b); 12) landslide: crown intercept (a), failure surface (b), dashed line when it is inferred.

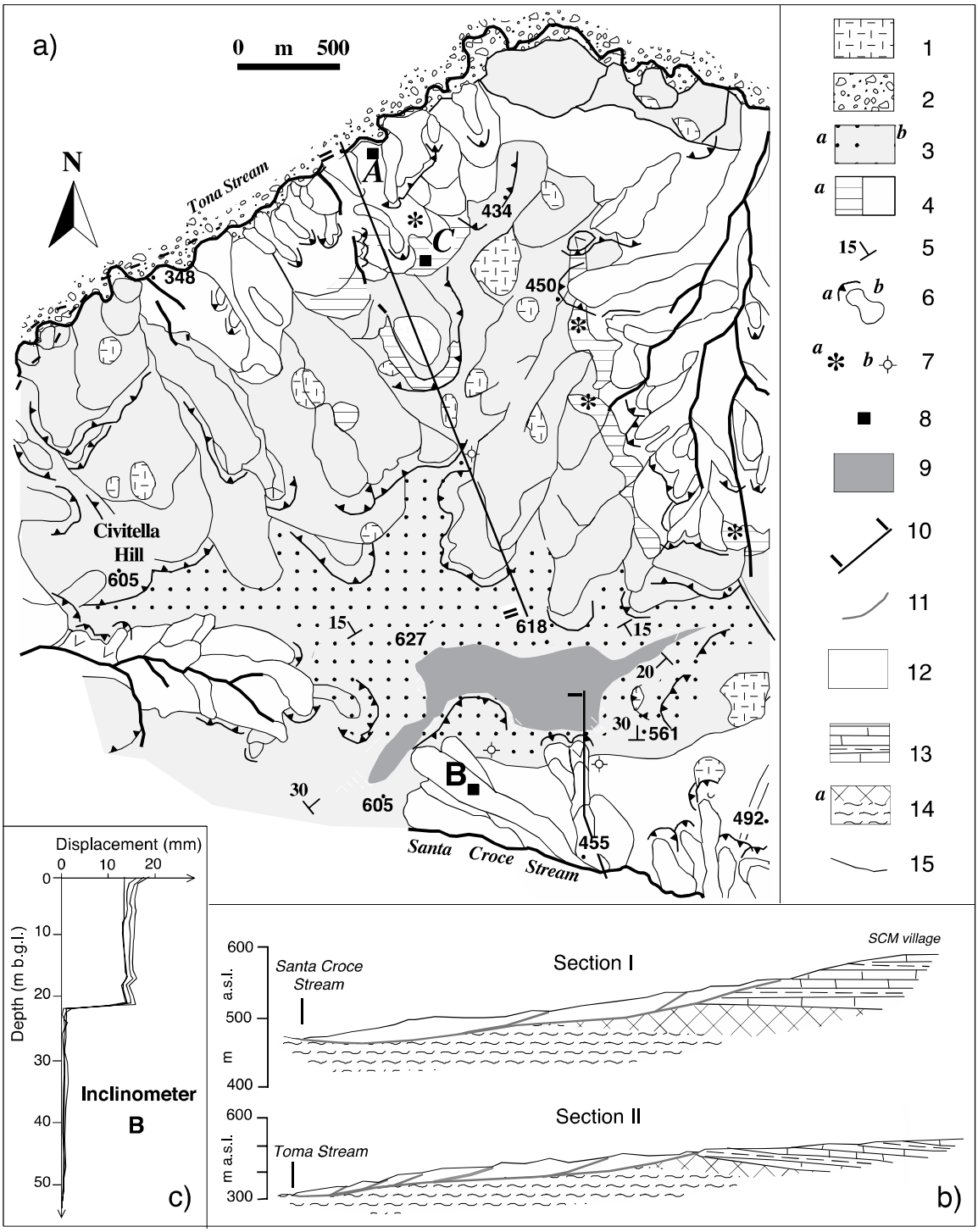


Fig. 6 Geological map (a) and sections (b) of Santa Croce di Magliano hill (after Melidoro et al. 2002), c) displacements, measured at depth within inclinometer B, after 1, 7, 8 and 9 months since the zero reading (after Cotecchia et al. 2007). Key - 1) colluvial deposits; 2) alluvial deposits; 3) Faeto Flysch stable (a) and landslide debris (b); 4) Red Flysch (SCM soils) with upper bentonite clays (a; BENT soils); 5) strata attitude; 6) landslide features (a-main scarp, b-body); 7) bentonite quarry (a) and spring (b); 8) location of the sampling areas and of the inclinometer (A: scaly clay blocks, B: undisturbed borehole samples and inclinometer, C: bentonite clay blocks); 9) Santa Croce di Magliano village; 10) lines of Sections I and II; 11) sliding surface; 12) landslide body; 13) FAE; 14) RF and bentonite (a) clayey strata, 15) stratigraphic contact.

	INTACT SOIL		DISCONTINUITY NATURE			DISCONTINUITY ORIENTATION[1]	DISCONTINUITY GEOMETRY		
	Main sediment fraction	*Undrained strength*[2]	*Type*	*Roughness*[3]	*State*		*Shape*[4]	*Continuity*[4]	*Intensity*[5]
	A	B	C	D	E	F	G	H	I
1	Clay °/*/**+/^	Mudstone	Depositional	Very rough	Fresh °/*/**/+^	Single*+	Planar°/*/**/+	Continuous+ 	Rare: <3m²/m³->1m³
2	Silt	Stiff clay °	Stress relief **	Rough	Slightly weathered °/*/**/+^	Few	Curved°/*	Many intersections °/*/**/^+ 	Very low: 3-10 m²/m³ 0.027-1 m³
3	Silty clay +^	Firm clay°/*/+/^	Shear induced °/*/**/+/^	Slightly rough	Highly weathered °/*	Many (random)°/**/^	Hinged°/*/^	Some intersections 	Low: 10-30 m²/m³ 0.001-0.027 m³
4	Clayey silt	Soft clay*/**/+^		Smooth °/*/**/^	Iron stained surfaces°		Folded°/*/**/^	Very few intersections 	Medium+: 30-100 m²/m³ 27-1000 cm³
5	Marly clay			Very smooth °/*	Coated		Conchoid^		High**/+^: 100-300 m²/m³ 1-27 cm³
6				Slickensided °/*/+/^					Very high°/*/^: >300m²/m³ - <1cm³

[1] With respect to the horizontal direction.

[2] After Morgenstern & Eigenbrod (1974) and BS 8004 (1986).

[3] Sandpaper grade (Fookes & Denness 1969); roughness classification (ISRM 1993).

[4] After Coffey & Partners in Walker et al. (1987).

[5] Area of discontinuities per unit volume (m^2/m^3) and/or average size (m^3, cm^3) of the intact peds/blocks (after Fookes & Denness 1969, modified).

.

Fig. 7 Characterisation chart for fissured clays; in grey are the F-IDs of the clays for which the applicability of the framework has been checked. For the clays in the slopes of reference in the paper, F-IDs: SEN scaly clay (°), SCM scaly clay (*), BENT (**), PD scaly clay I6 (^), PD scaly clay I5-I4 (+).

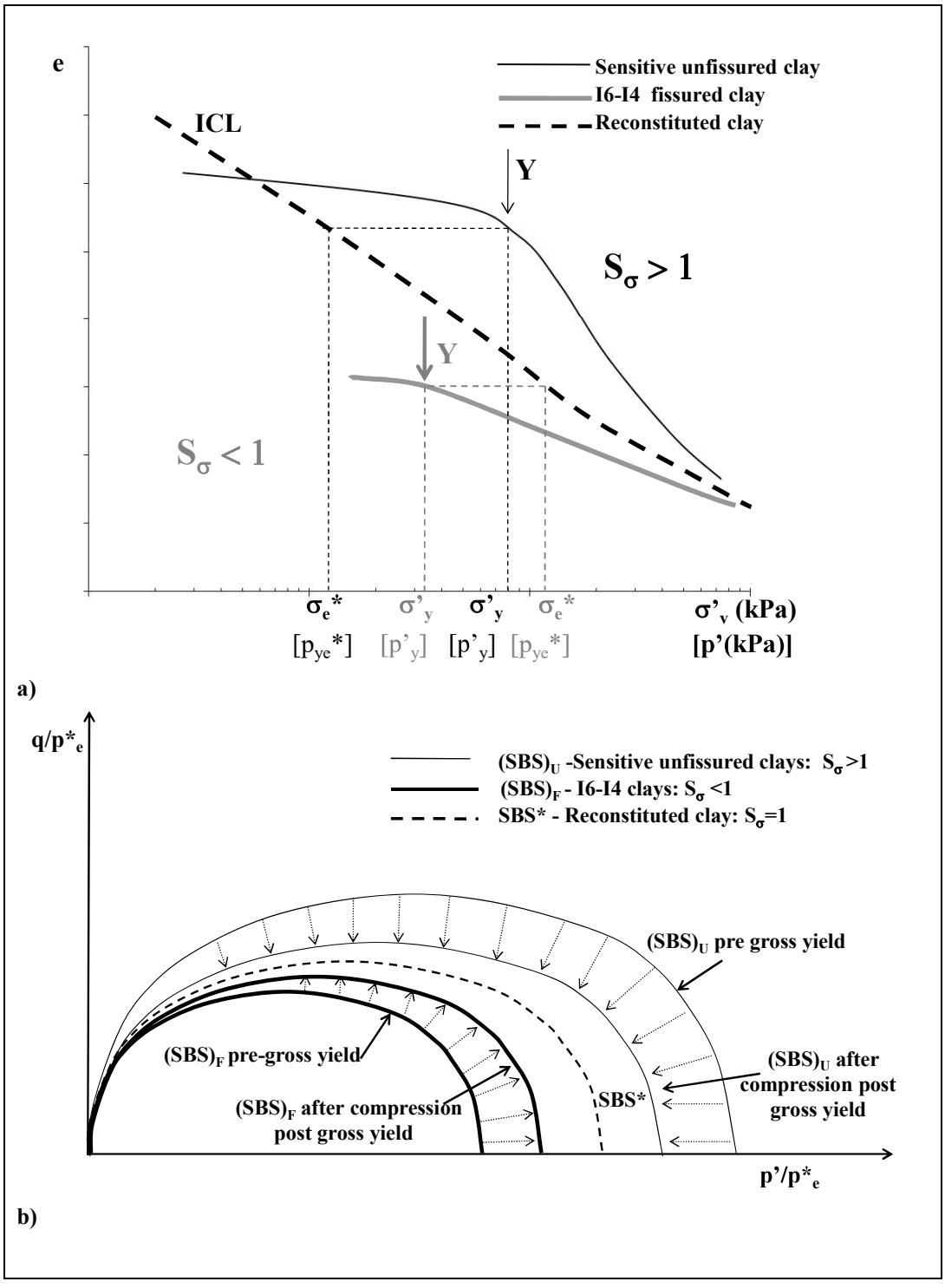


Fig. 8 Natural fissured clay, sensitive unfissured clay and reconstituted clay: framework of a) compression and b) shearing behaviour (after Vitone and Cotecchia 2011, modified)

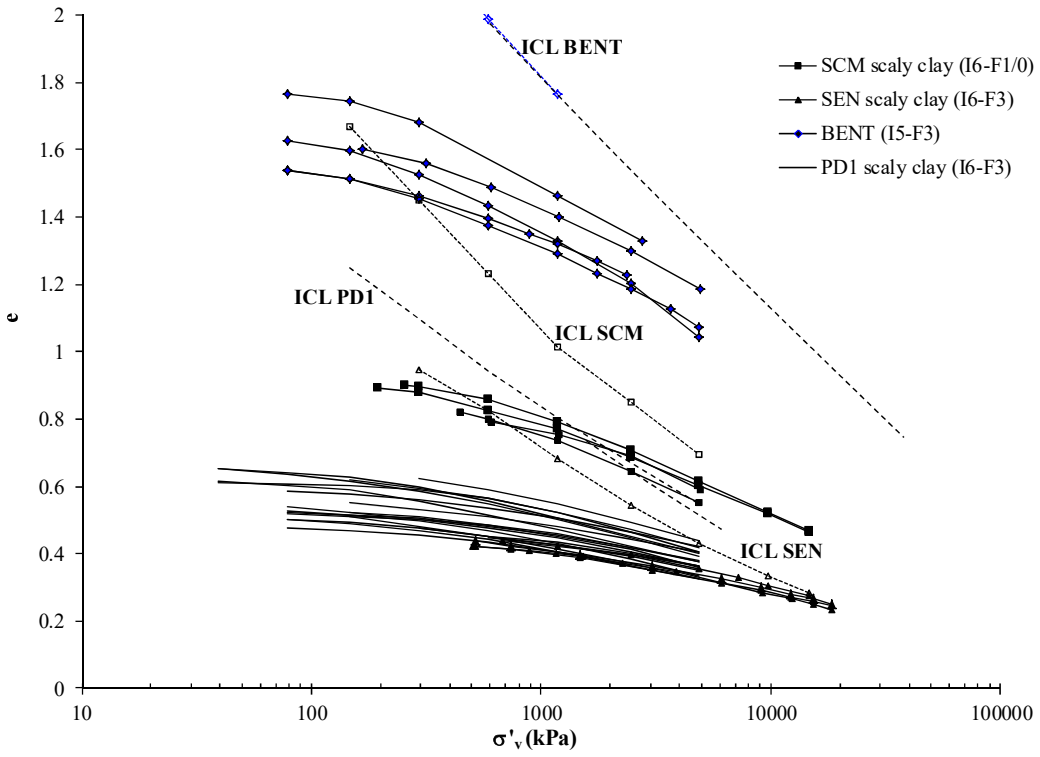


Fig. 9 Natural (continuous lines and full symbols) fissured clays and reconstituted (dashed lines and empty symbols): oedometer compression curves; data from Vitone & Cotecchia (2011) and new data (PD scaly clays).

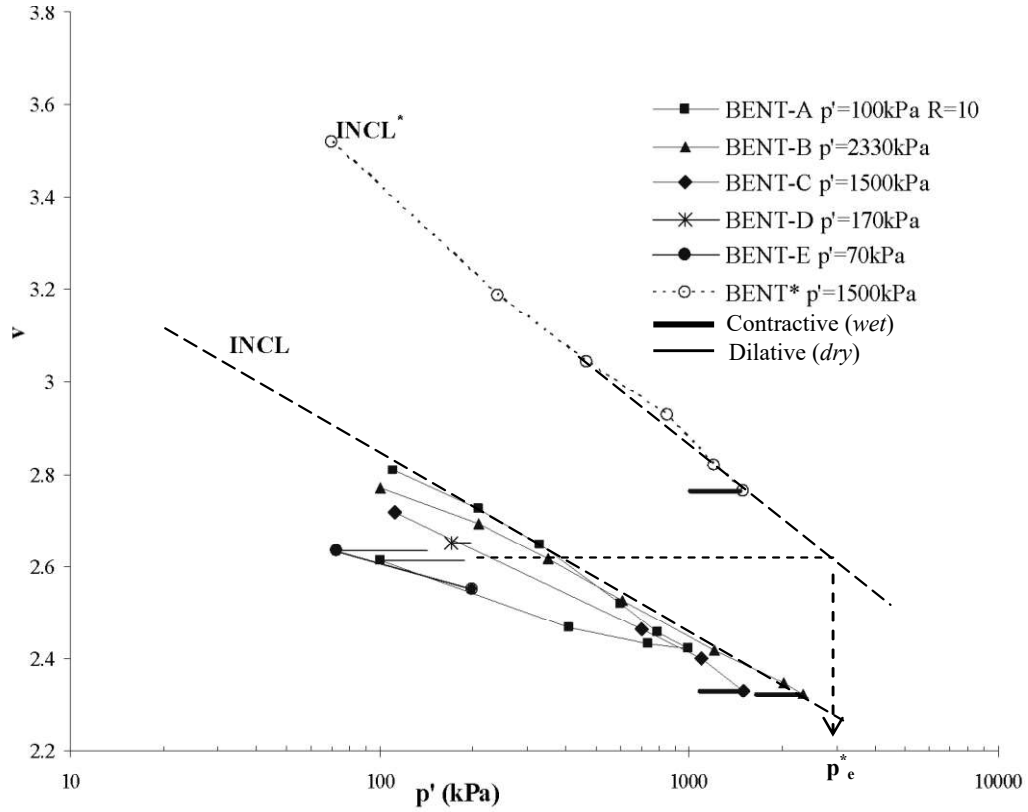


Fig. 10 Natural and reconstituted BENT: isotropic compression and undrained shear state paths.

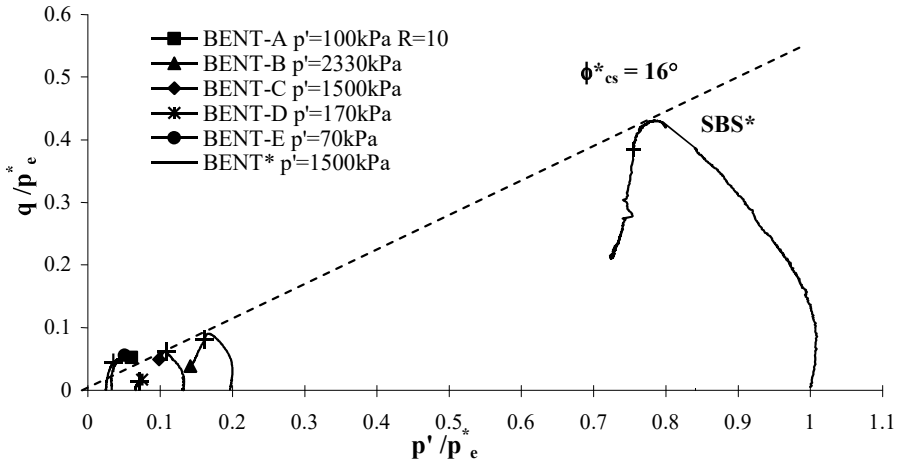


Fig. 11 Natural and reconstituted BENT: undrained stress paths normalized for volume (see Fig. 10).

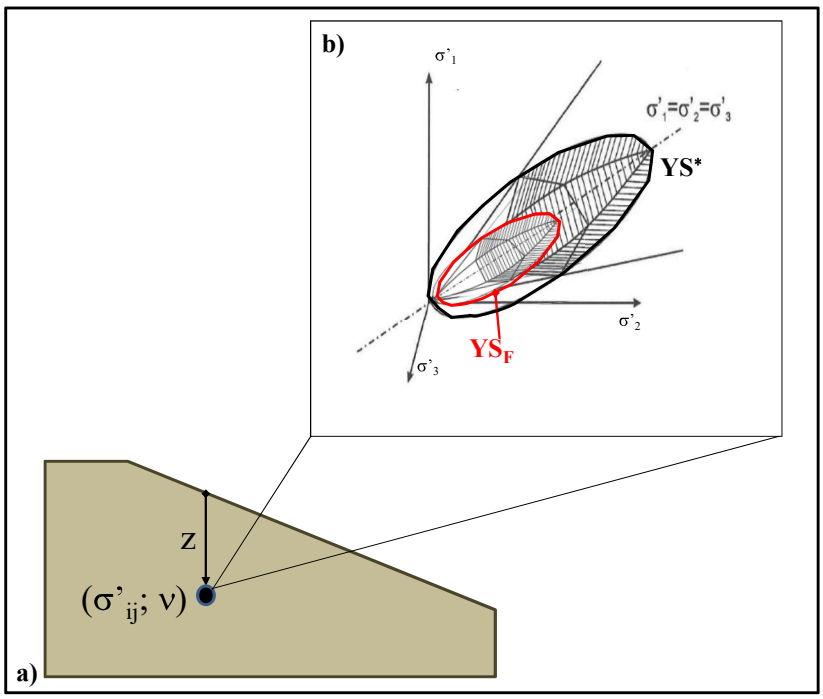


Fig. 12 Conceptual scheme representing the influence of fissuring on the slope stability. In the general stress space (b), the yield surface of the fissured clay, YS_F, and of the reconstituted clay, YS*, are compared. The asterisk, *, is used for the reconstituted clay.

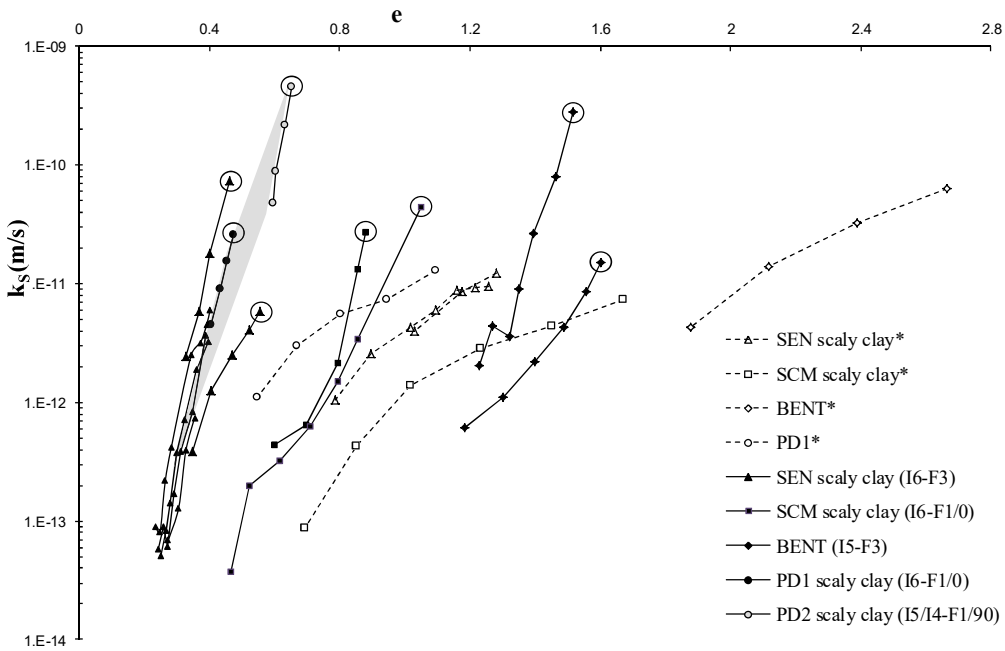


Fig. 13 Reconstituted and natural fissured clays: permeability values measured in the laboratory. Dashed lines refer to the reconstituted clay (*) and circles are used for the k_s-e states of the samples in the slopes. The grey area represents the permeability spindle found for PD1 and PD2 clays.

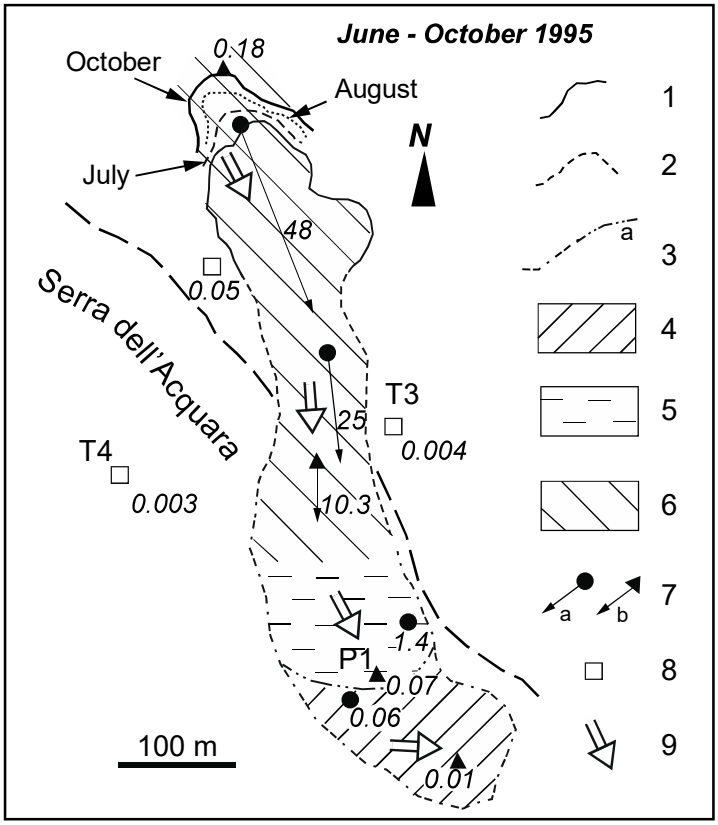


Fig. 14 Horizontal displacement rates (m/month) of the Vadoncello landslide. Key: 1) area A; 2) area B; 3) area C and front of the earth-flow (a); 4) 0.02-0.2 m/month; 5) 0.4-10 m/month; 6) 10-20 m/month; 7) maximum (a) and minimum (b) rates; 8) GPS control stations; 9) average displacement direction (after EEC Project 1996, Santaloia et al. 2001, modified).

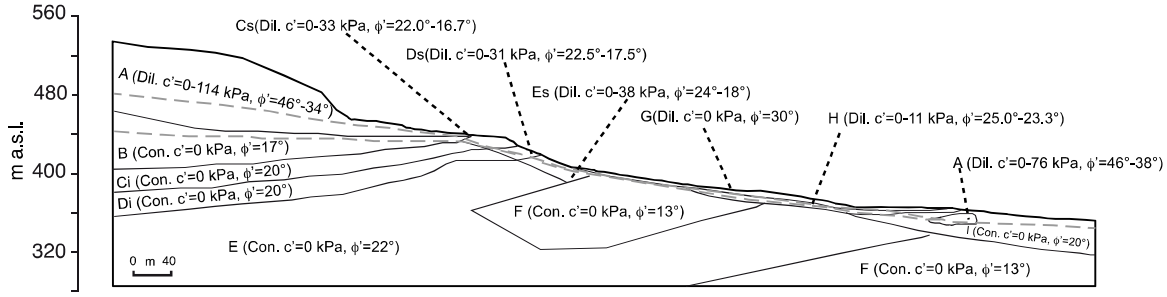


Fig. 15 Vadoncello slope: geotechnical model (Dil: dilative, Con: contractive soil behaviour); the dashed lines represent the water tables of the two seepage domains modelled in the slope (after Cotecchia et al. 2000).

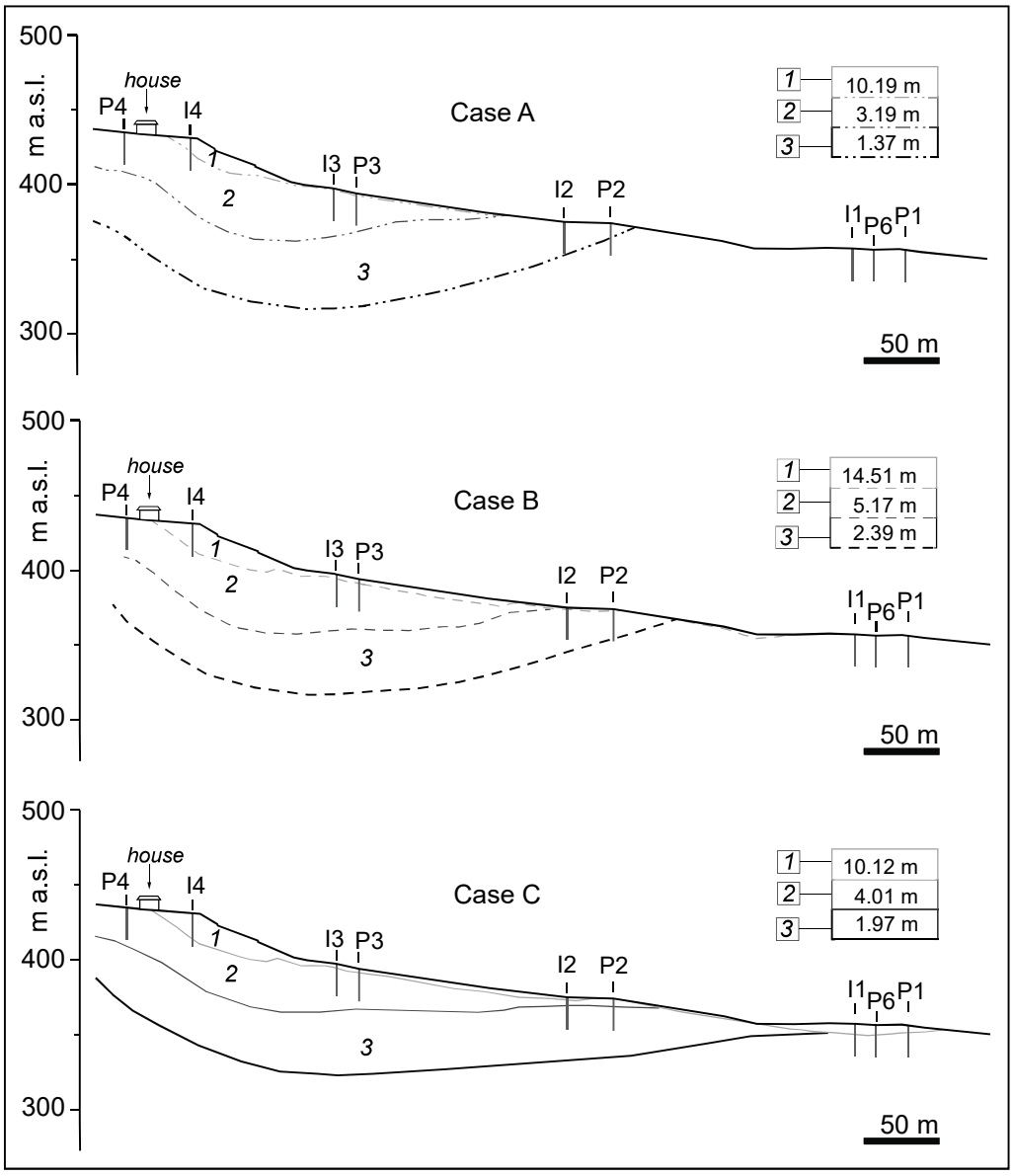


Fig. 16 Vadoncello slope: results of the numerical analysis; areas 1, 2 and 3 are location of quasi-uniform displacement values; the values are shown in the legend for: A - no seepage and no toe translation; B - seepage and no toe translation; C- seepage and toe translation; boreholes equipped with inclinometer (I); boreholes equipped with piezometers (P) (after Cotecchia et al. 2000, modified).

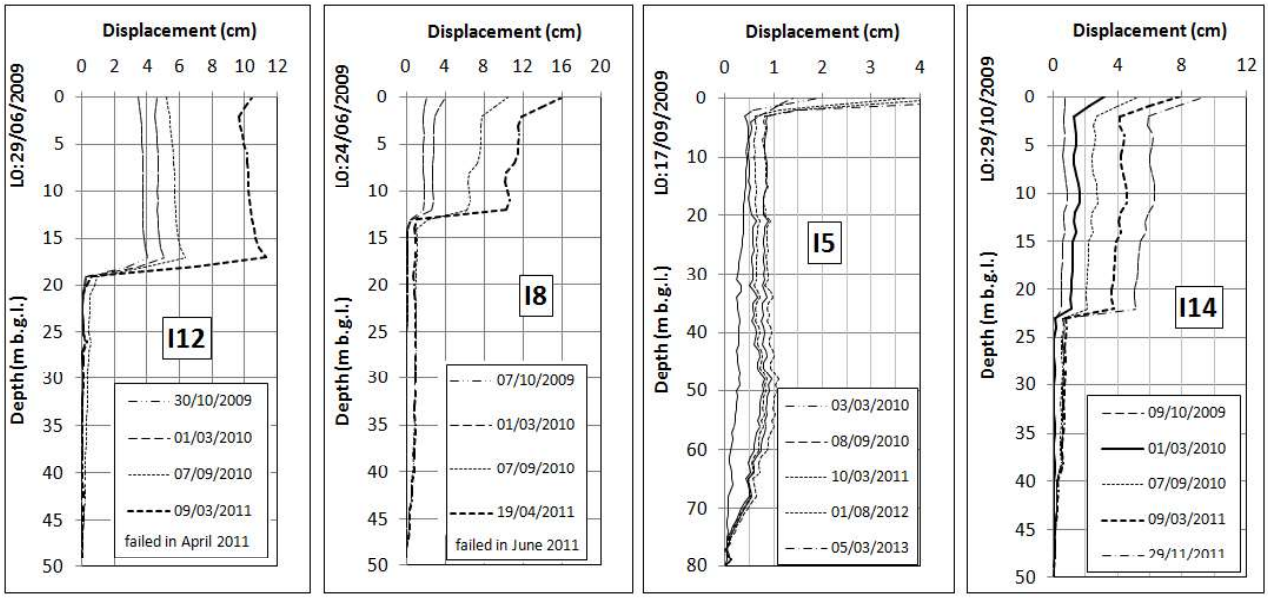


Fig. 17 Cumulative displacement inclinometer profiles within the Pisciolo slope. Zero reading in 2009 (L0 in the graphs); location of inclinometers in Fig. 5 (after Cotecchia et al. 2012).

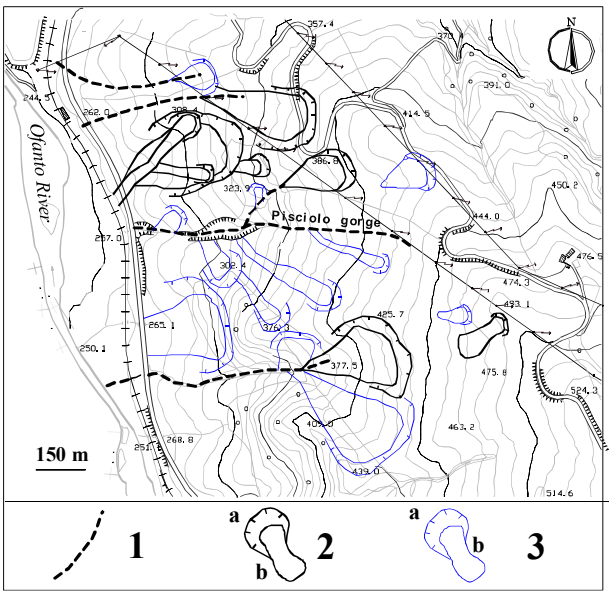


Fig. 18 Geomorphological map of the Pisciolo landslide basin (from 1955 aerial photos). Key: (1) deep ditch; (2) active and (3) inactive deep landslides: a-crown, b-body (after Cotecchia et al. 2012).

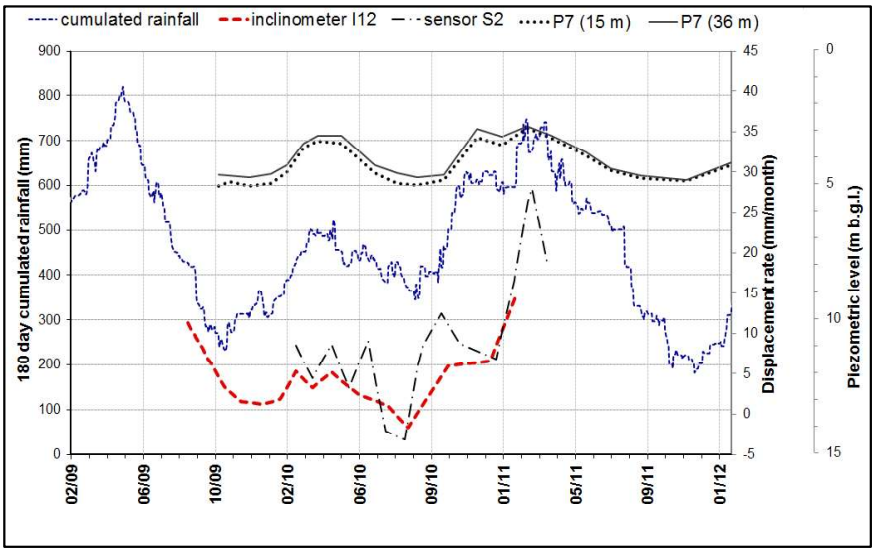


Fig. 19 Displacement rates at 19 m depth down inclinometer I12 and at ground surface (GPS sensor S2); piezometric levels at 15 m and 36 m b.g.l. down borehole P7 and 180 day cumulated rainfall (the location of the monitoring points in Fig. 5).

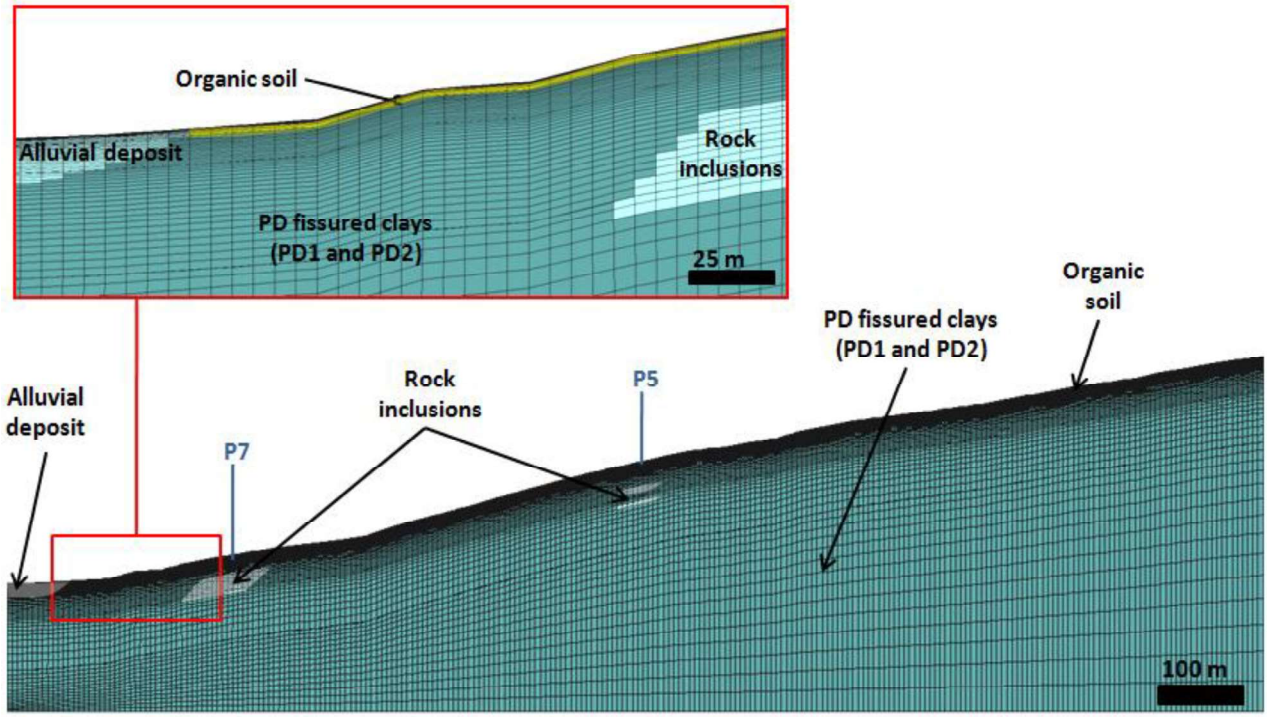


Fig. 20 Numerical model of section II across the Pisciolo hillslope; the line of section is shown in Fig. 5b.

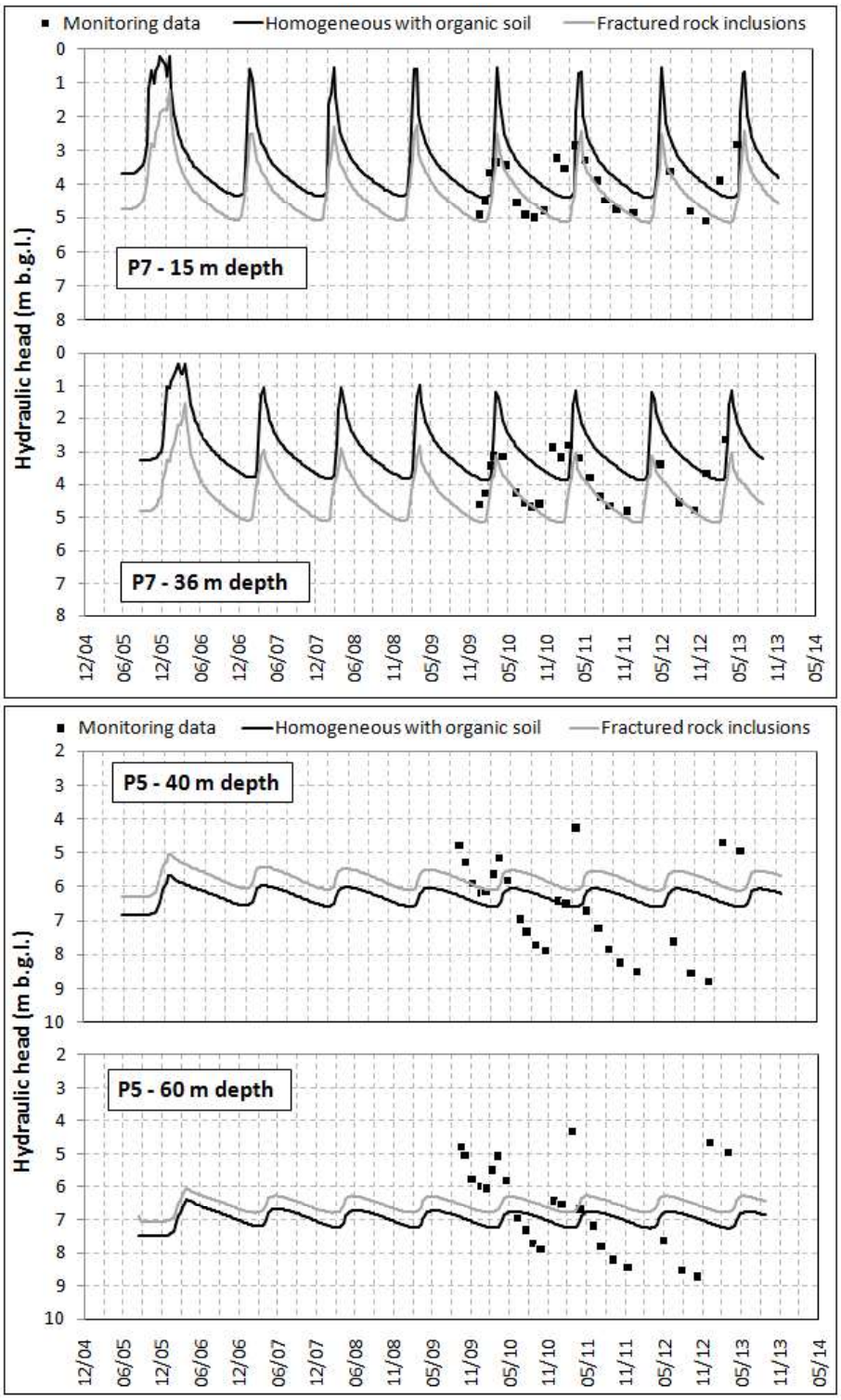


Fig. 21 Measured hydraulic heads (down boreholes P5 and P7) compared to those resulting from the numerical analyses of the model whose numerical mesh is shown in Fig. 20 (section II of the Pisciolo hillslope; line of section in Fig. 5b).

Table 1 Clays of reference for the present study: fissuring identities, composition and physical properties. Key: CF: clay fraction; SF: sand fraction; PI: Plasticity index; A: activity; e_0: initial void ratio; USCS Class: classification according to the Unified Soil Classification System (ASTM 1985)

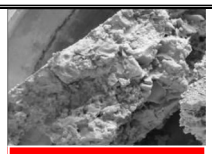
SLOPE	CLAY										
	Name	Fissuring characterisation *F-ID*	Sampling		Composition and physical properties						
			Type	Depth range (m b.g.l.)	CF %	SF %	PI %	A -	e_0 -	CI -	USCS Class
Santa Croce di Magliano (SCM)	SCM scaly clay	 **F1-I6** A1; B3-4; C3; D4-6; E1-3; F1; G1-4; H2; I6	block	3.0	91	9	55	0.6	0.88-1.05	1.1	CH
			borehole	54.4	73	-	28	0.4	0.54-0.64	1.9	CH
	BENT	 **F3-I5** A1; B4; C2-3; D4; E1-2; F3; G1, G4; H2; I5	block	18.0	66	2	86	1.3	1.55-1.79	0.9	CH
Vadoncello (SEN)	SEN scaly clay	 **F3-I6** A1; B2-3; C3; D4-6; E1-4; F3; G1-4; H2; I6	borehole	16.0-52.3	36-68	4-18	23-54	0.4-0.8	0.43-0.51	1.0-1.5	CH-CL
Pisciolo (PI)	PD2	 **F1-I5/I4** A1, A3; B3-4; C3; D6; E1-2; F1; G1; H1-2; I5/I4	borehole	6.0-80.0	19-55	16-26	24-44	0.5-1.0	0.41-0.69	1.0-1.6	CH
	PD1	 **F3-I6** A1, A3; B3-4; C3; D4, D6; E1-2; F3; G3-5; H2; I6		9.4-80.1	36-70	5-16	38-67	0.6-1.3	0.43-0.81	1.0-1.3	CH

Table 2 Values of friction angles of the fissured and reconstituted clays. Key: data from (a) CIU triaxial tests; (b) Bromhead ring shear tests; (c) reversal direct shear tests; n.d. data not determined

SOIL TYPE	SHEAR TEST RESULTS
SE scaly clay	$\phi'_{peak} \approx 18.5°\text{-}20.5°$ (*dry* side, R≈ 3) – (a) $\phi'_{post\text{-}peak} = 12°\text{-}15°$ – (a) $\phi'_{r} \approx 5°$ – (b) $\phi^{*}_{cs} \approx 19°$ – (a)
SCM scaly clay	$\phi'_{peak} \approx 13°\text{-}22°$ (*dry* side, R≈ 2.5-20) – (a) $\phi'_{post\text{-}peak} = 9°\text{-}12°$ – (a) $\phi'_{r} \leq 9°$ – (c) $\phi^{*}_{cs} \approx 18°$ – (a)
BENT	$\phi'_{peak} \approx 16°\text{-}28°$ (*dry* side, R≈3-10) – (a) $\phi'_{post\text{-}peak} = 12°\text{-}27°$ – (a) $\phi'_{r} \approx 5°$ – (b) $\phi^{*}_{cs} \approx 16°$ – (a)
PD1and PD2 scaly clay	$\phi'_{peak} \approx 21°\text{-}25°$ (*dry* side, R≈3-10) – (a) $\phi'_{post\text{-}peak} = 13°\text{-}20°$ – (a) $\phi'_{r} \approx$ n.d. $\phi^{*}_{cs} \approx 18°$ – (a)

Fig. 1
Click here to download Figure: Fig1 Final.eps

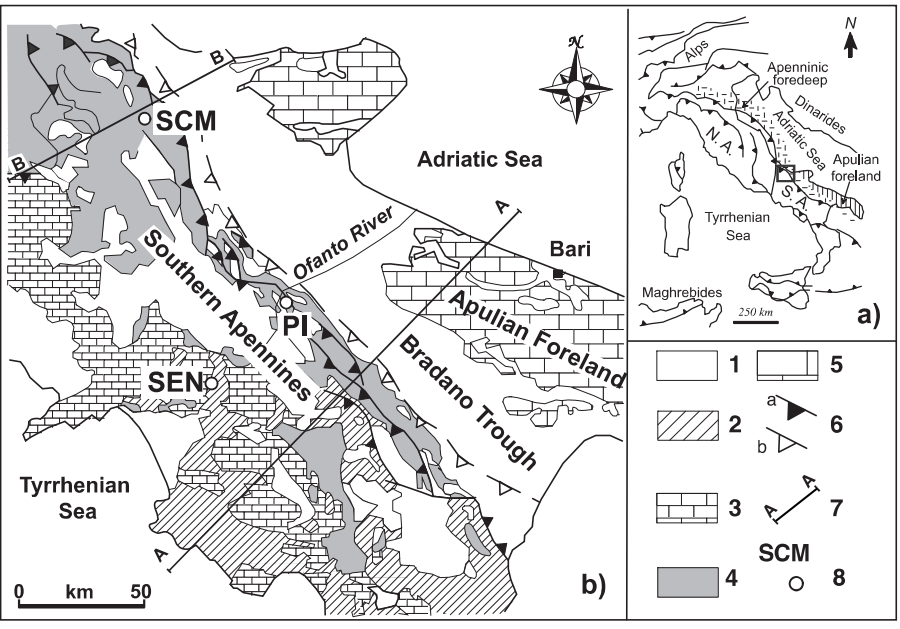


Fig. 2
Click here to download Figure: Fig2 Final.eps

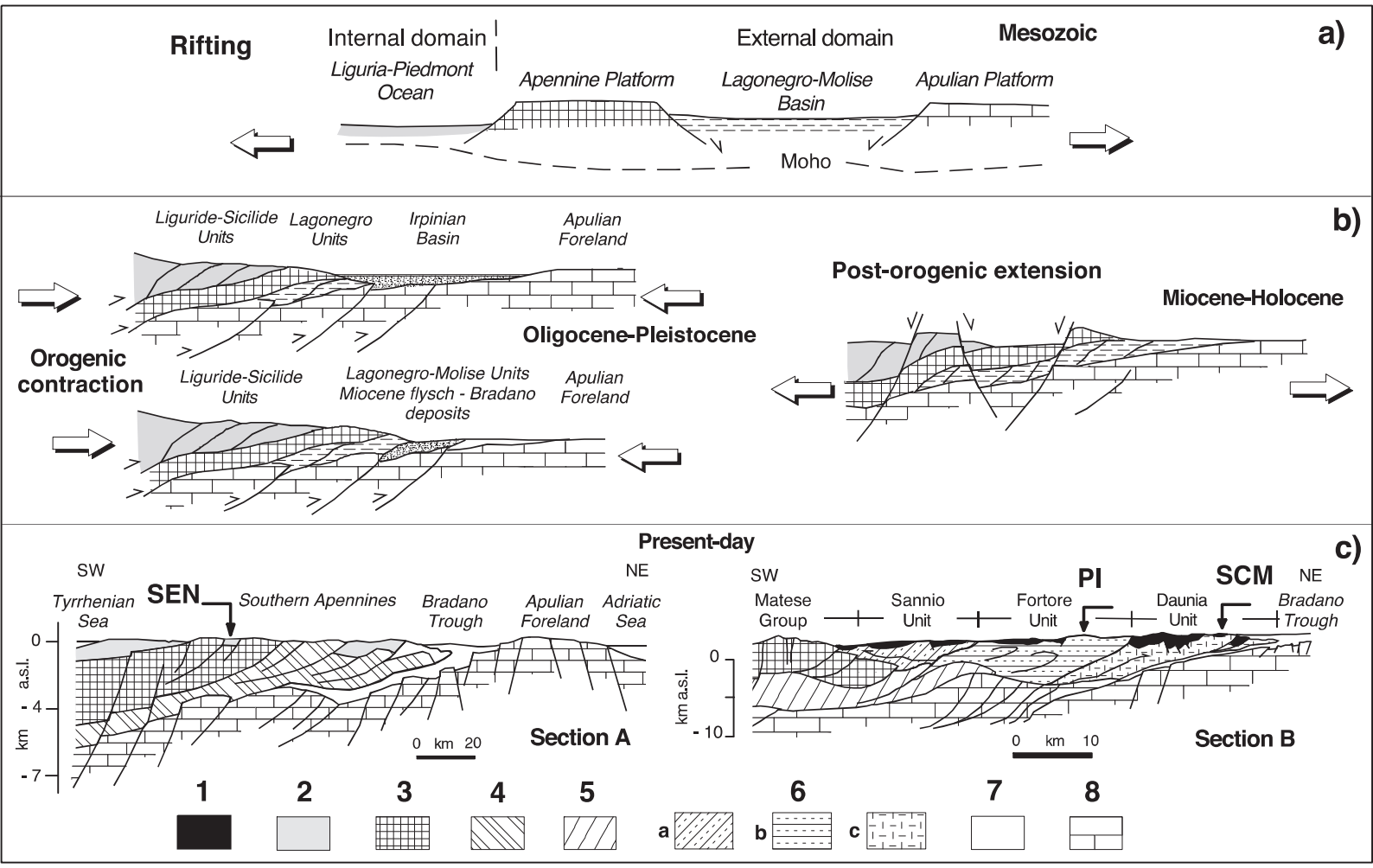


Fig. 3
Click here to download Figure: Fig3.eps

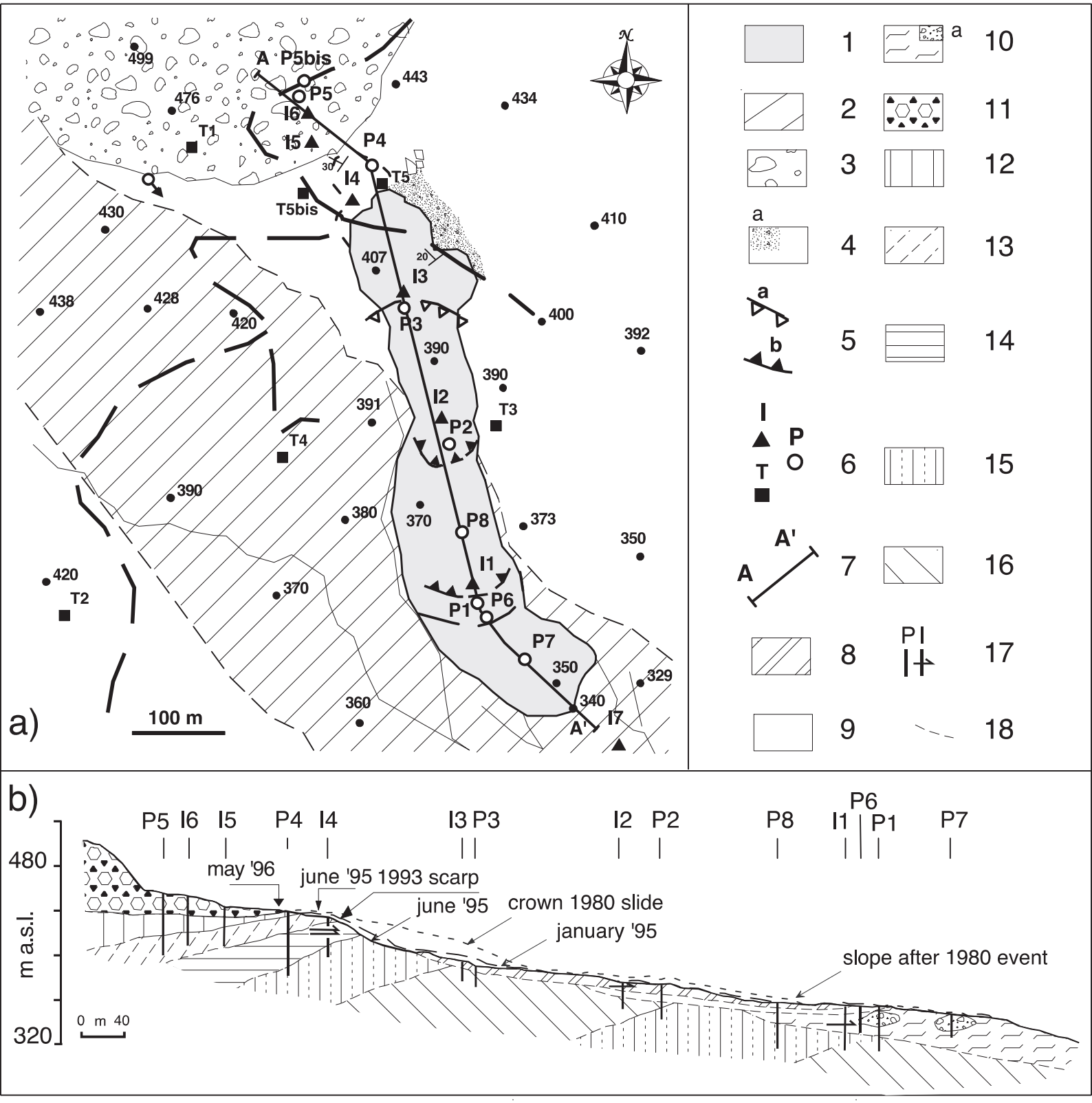


Fig. 4
Click here to download Figure: Fig4 Final.eps

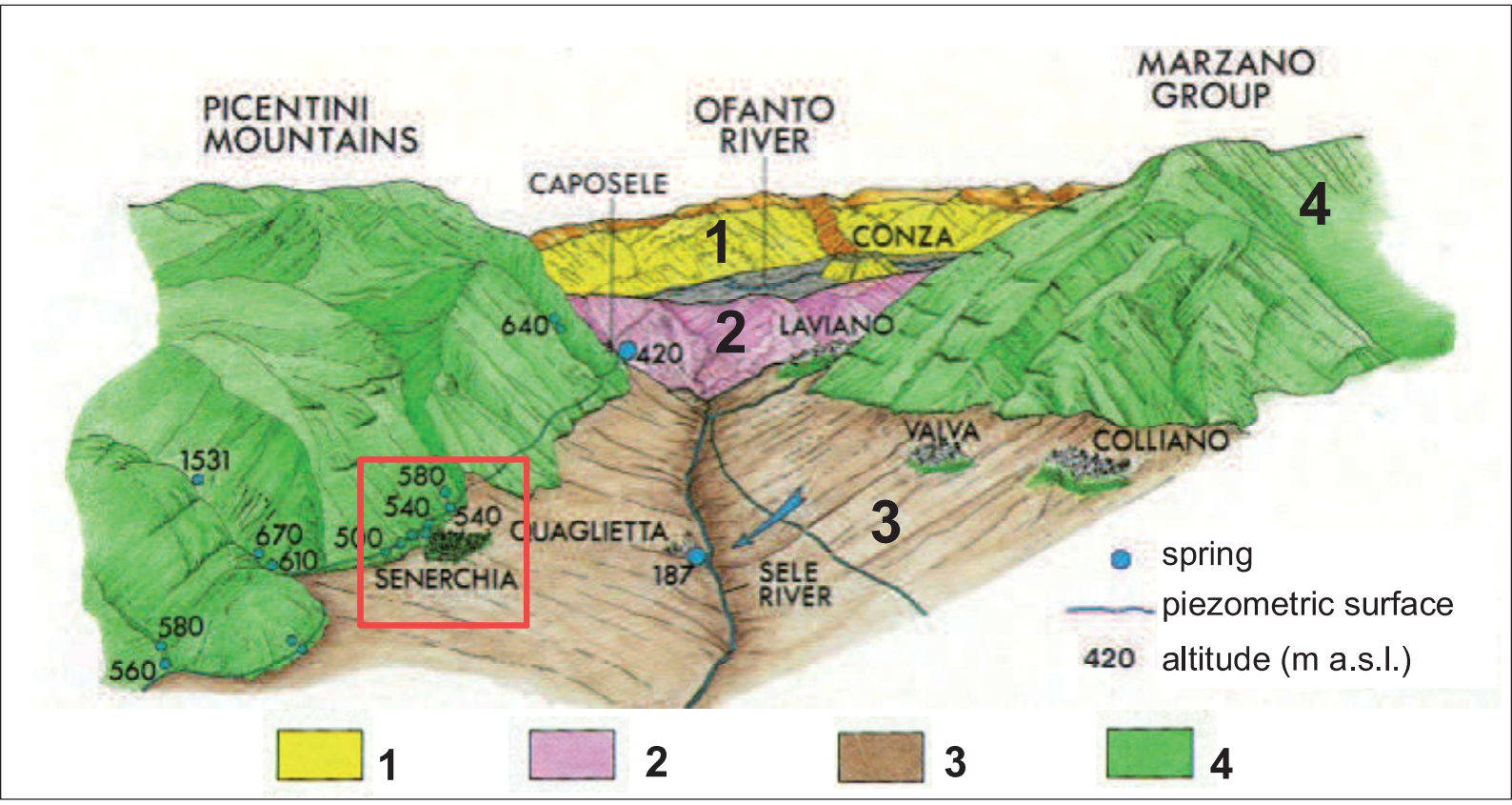


Fig. 5
Click here to download Figure: Fig5 Final.eps

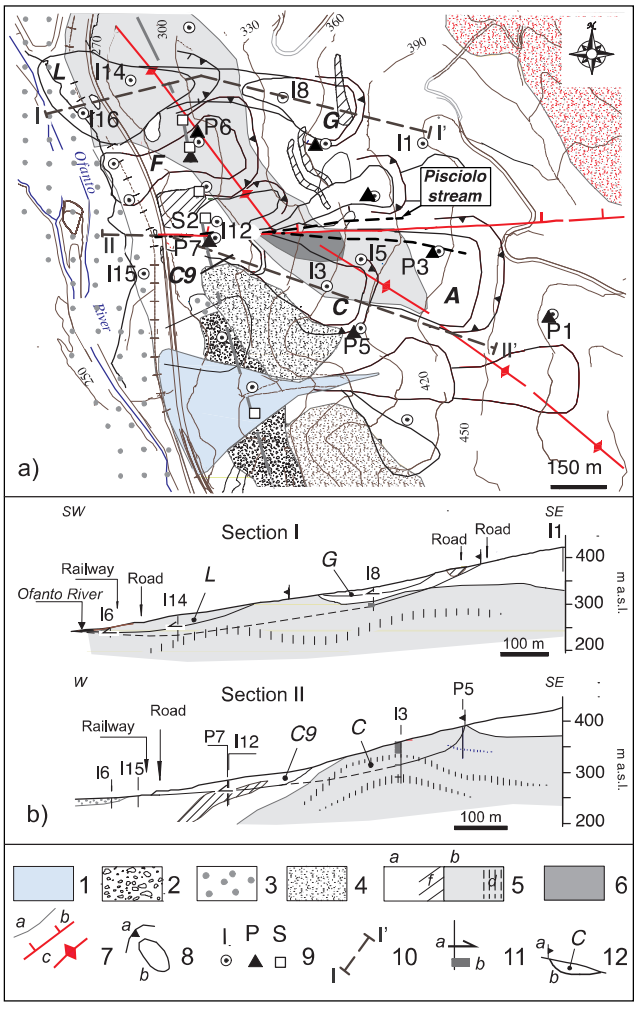


Fig. 6
Click here to download Figure: Fig6 Final.eps

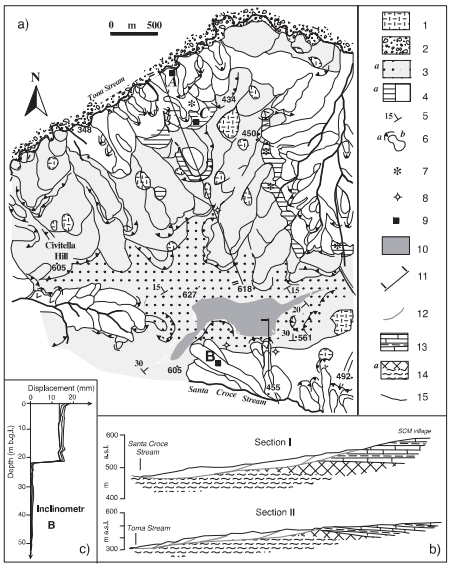


Fig. 7
Click here to download high resolution image

	INTACT SOIL		DISCONTINUITY NATURE			DISCONTINUITY ORIENTATION[1]	DISCONTINUITY GEOMETRY		
	Main sediment fraction	*Undrained strength*[2]	*Type*	*Roughness*[3]	*State*		*Shape*[4]	*Continuity*[4]	*Intensity*[5]
	A	B	C	D	E	F	G	H	I
1	Clay	Mudstone	Depositional	Very rough	Fresh	Single	Planar	Continuous	Rare: <3m²/m³ -> 1m³
2	Silt	Stiff clay	Stress relief	Rough	Slightly weathered	Few	Curved	Many intersections	Very low: 3-10 m²/m³ 0.027-1 m³
3	Silty clay	Firm clay	Shear induced	Slightly rough	Highly weathered	Many (random)	Hinged	Some intersections	Low: 10-30 m²/m³ 0.001-0.027 m³
4	Clayey silt	Soft clay		Smooth	Iron stained surfaces		Folded	Very few intersections	Medium: 30-100 m²/m³ 27-1000 cm³
5	Marly clay			Very smooth	Coated		Conchoid		High: 100-300 m²/m³ 1-27 cm³
6				Slickensided					Very high: >300m²/m³ - <1cm³

[1] With respect to the horizontal direction.

[2] After Morgenstern & Eigenbrod (1974) and BS 8004 (1986).

[3] Sandpaper grade (Fookes & Denness 1969); roughness classification (ISRM 1993).

[4] After Coffey & Partners in Walker et al. (1987).

[5] Area of discontinuities per unit volume (m^2/m^3) and/or average size (m^3, cm^3) of the intact peds/blocks (after Fookes & Denness 1969, modified).

Fig. 8
Click here to download high resolution image

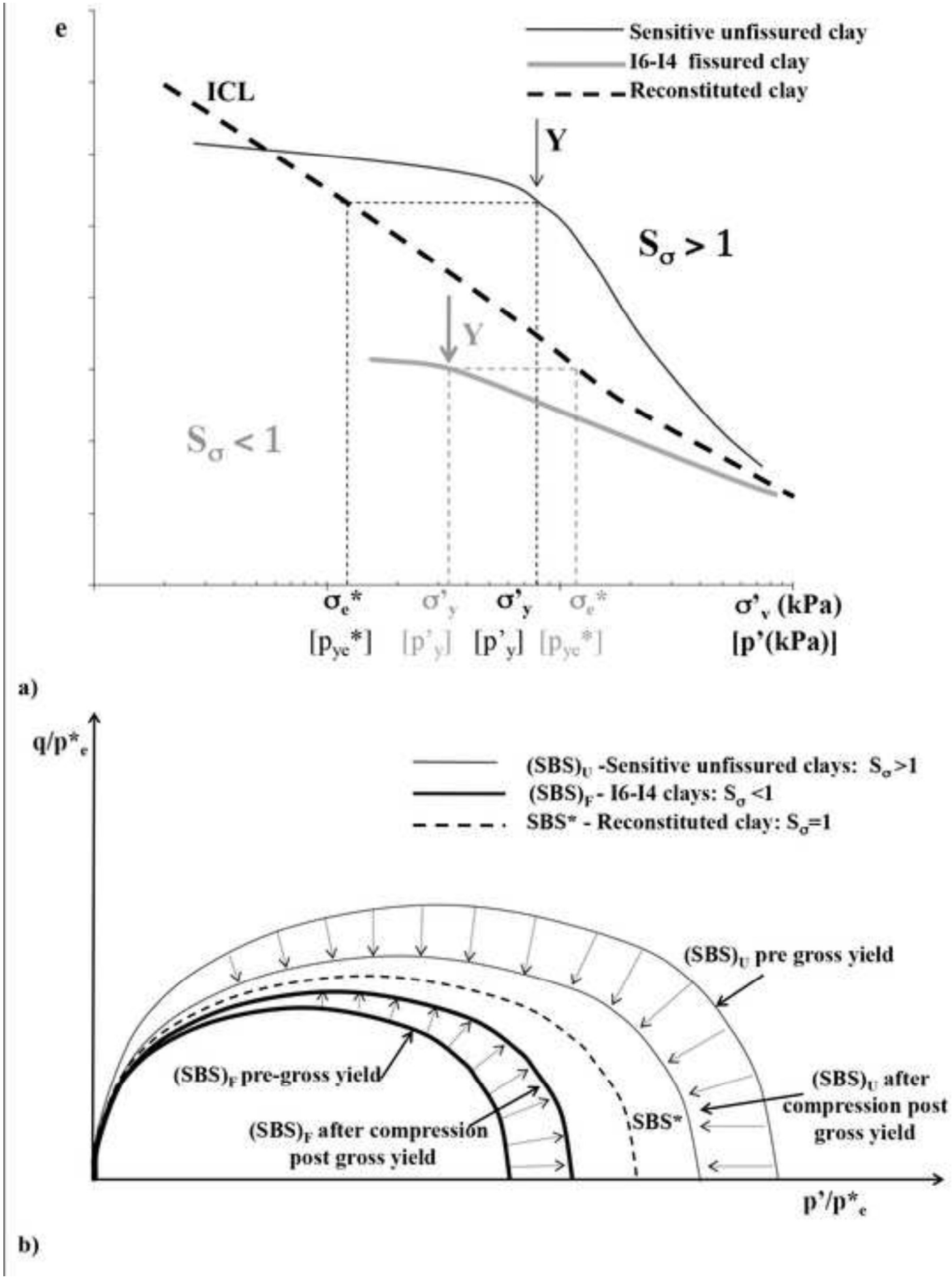


Fig. 9
Click here to download high resolution image

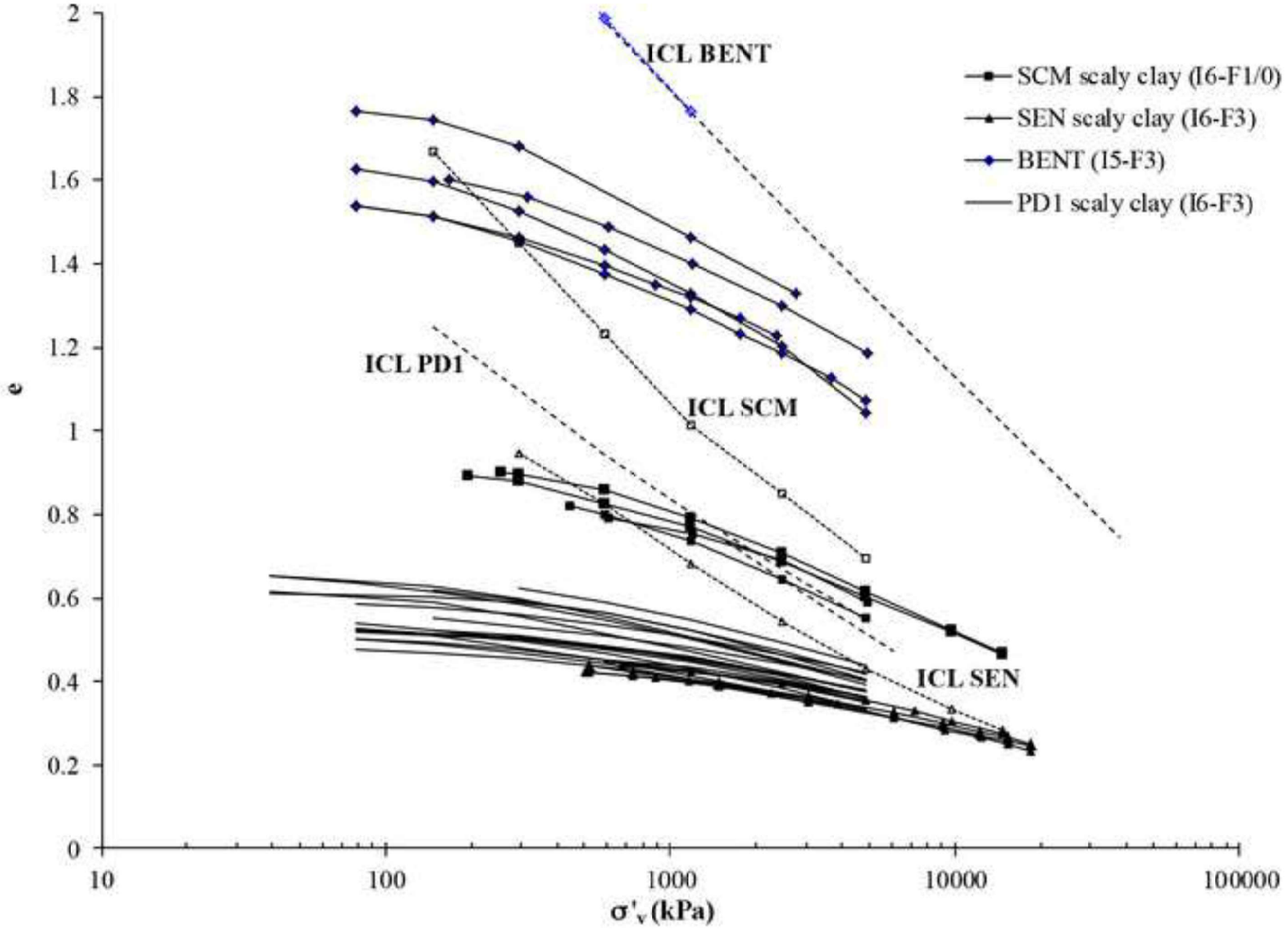


Fig. 10
Click here to download high resolution image

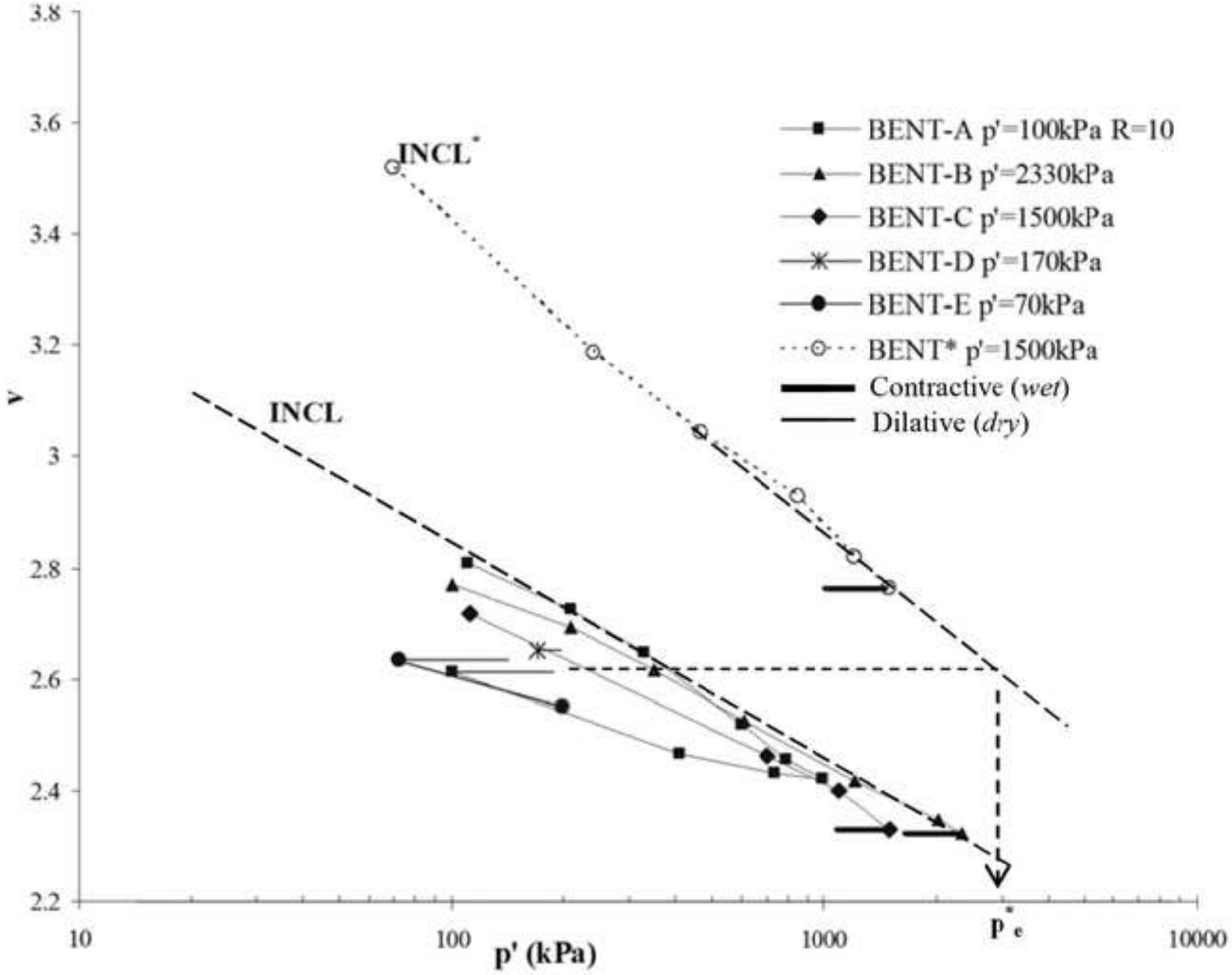


Fig. 11
Click here to download high resolution image

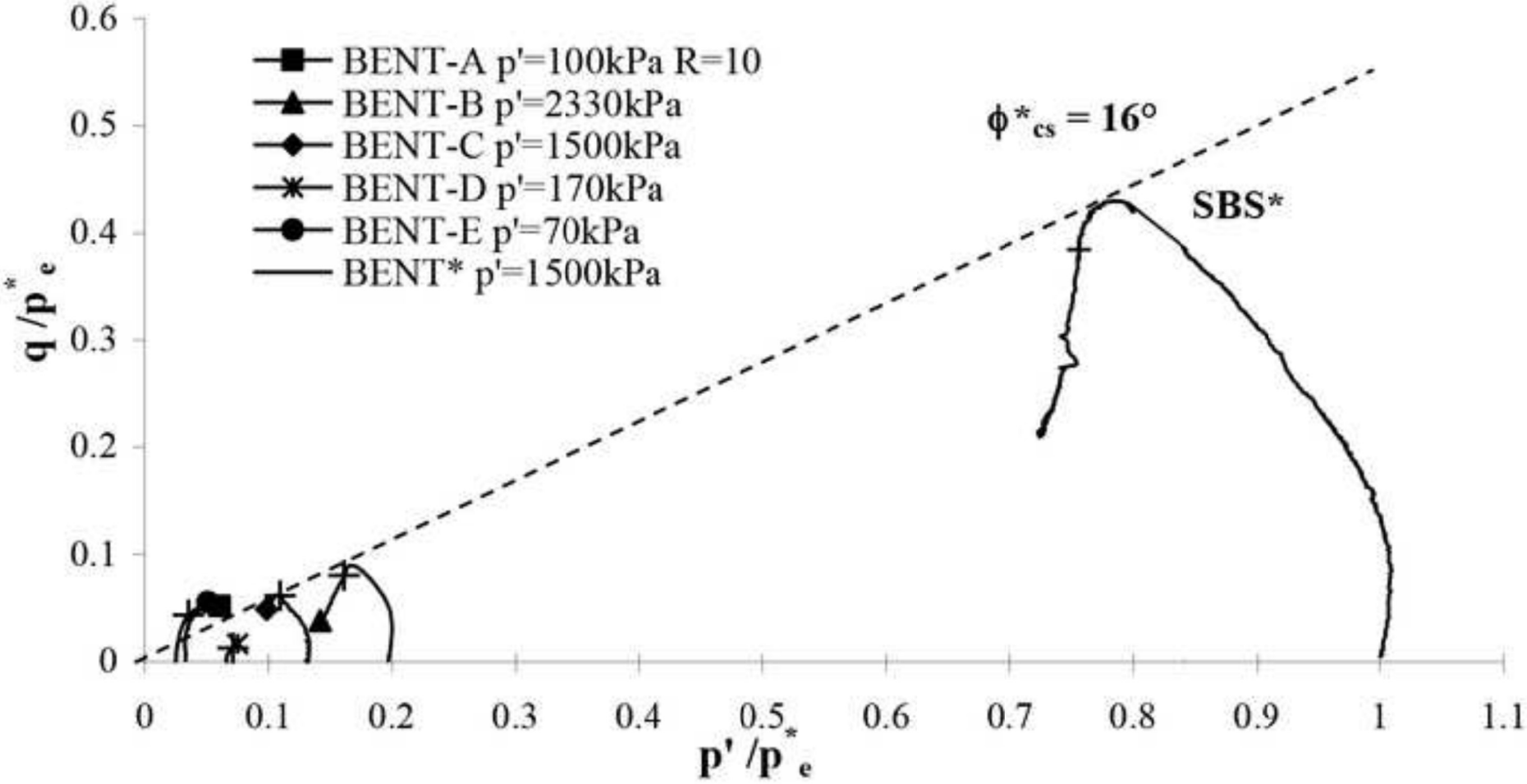


Fig. 12
Click here to download high resolution image

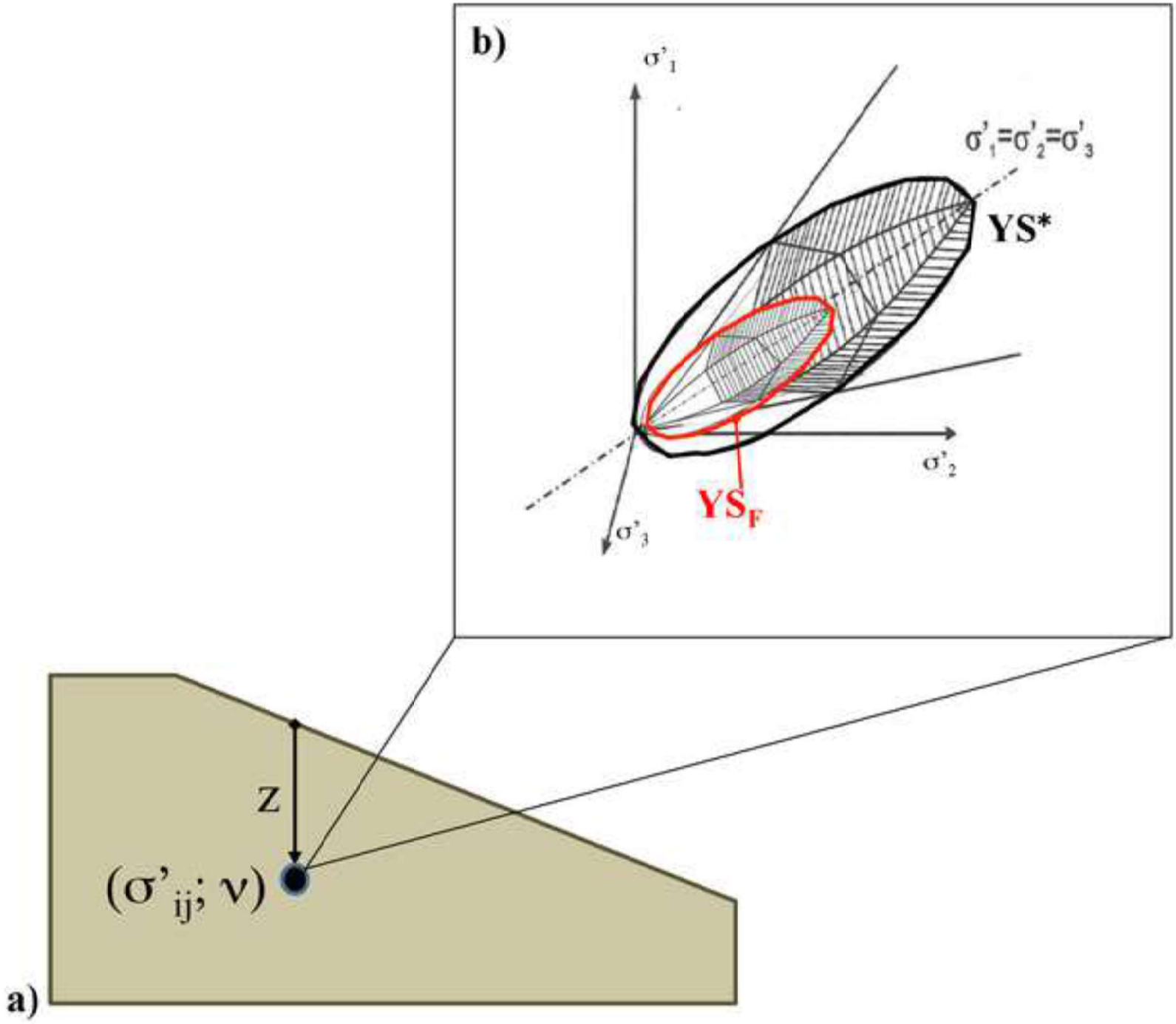


Fig. 13
Click here to download high resolution image

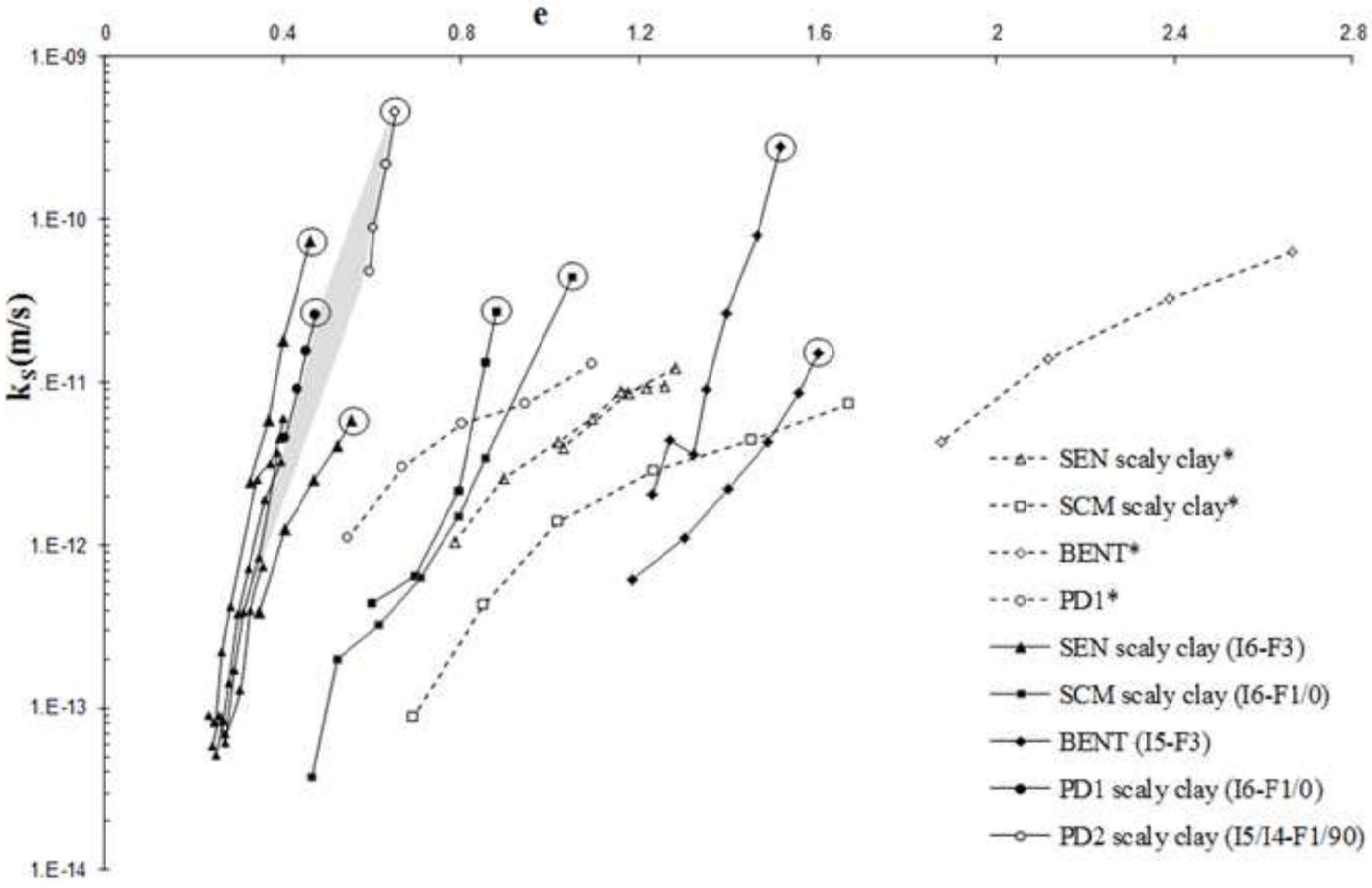


Fig. 14
Click here to download Figure: Fig14 Final.eps

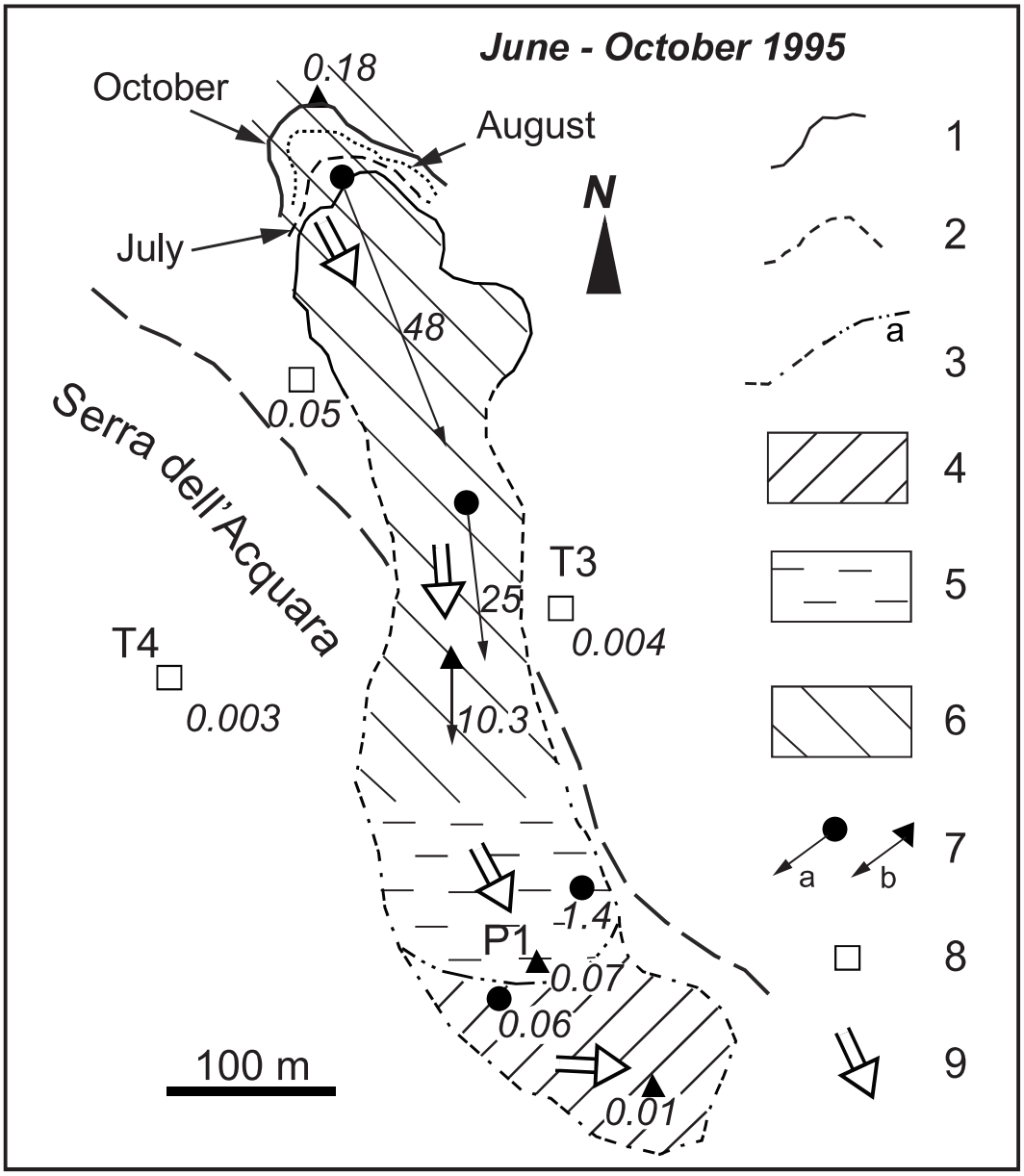


Fig. 15
Click here to download Figure: Fig15 Final.eps

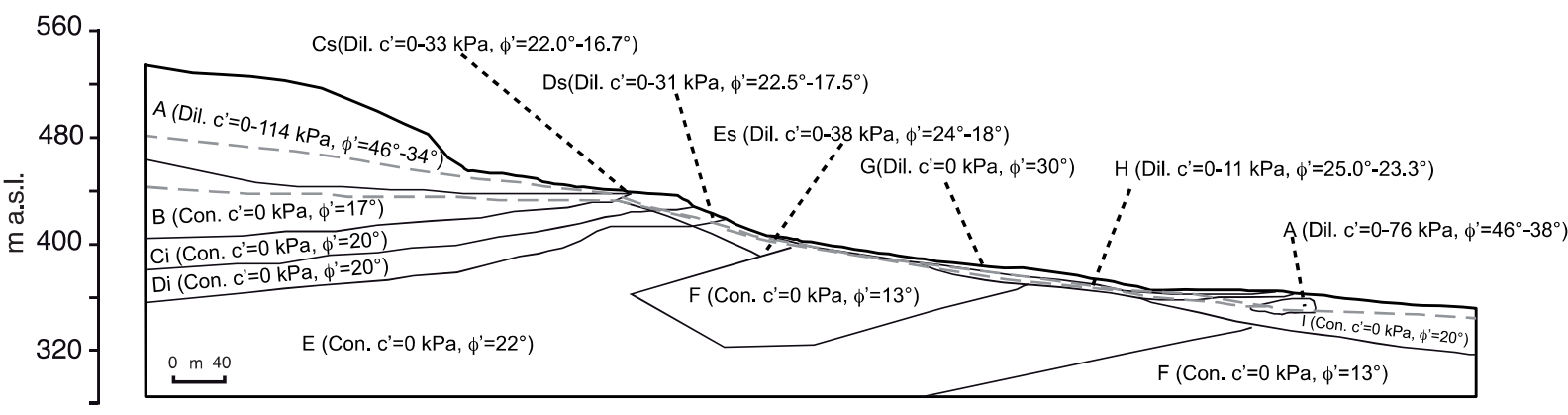


Fig. 16
Click here to download Figure: Fig16 Final.eps

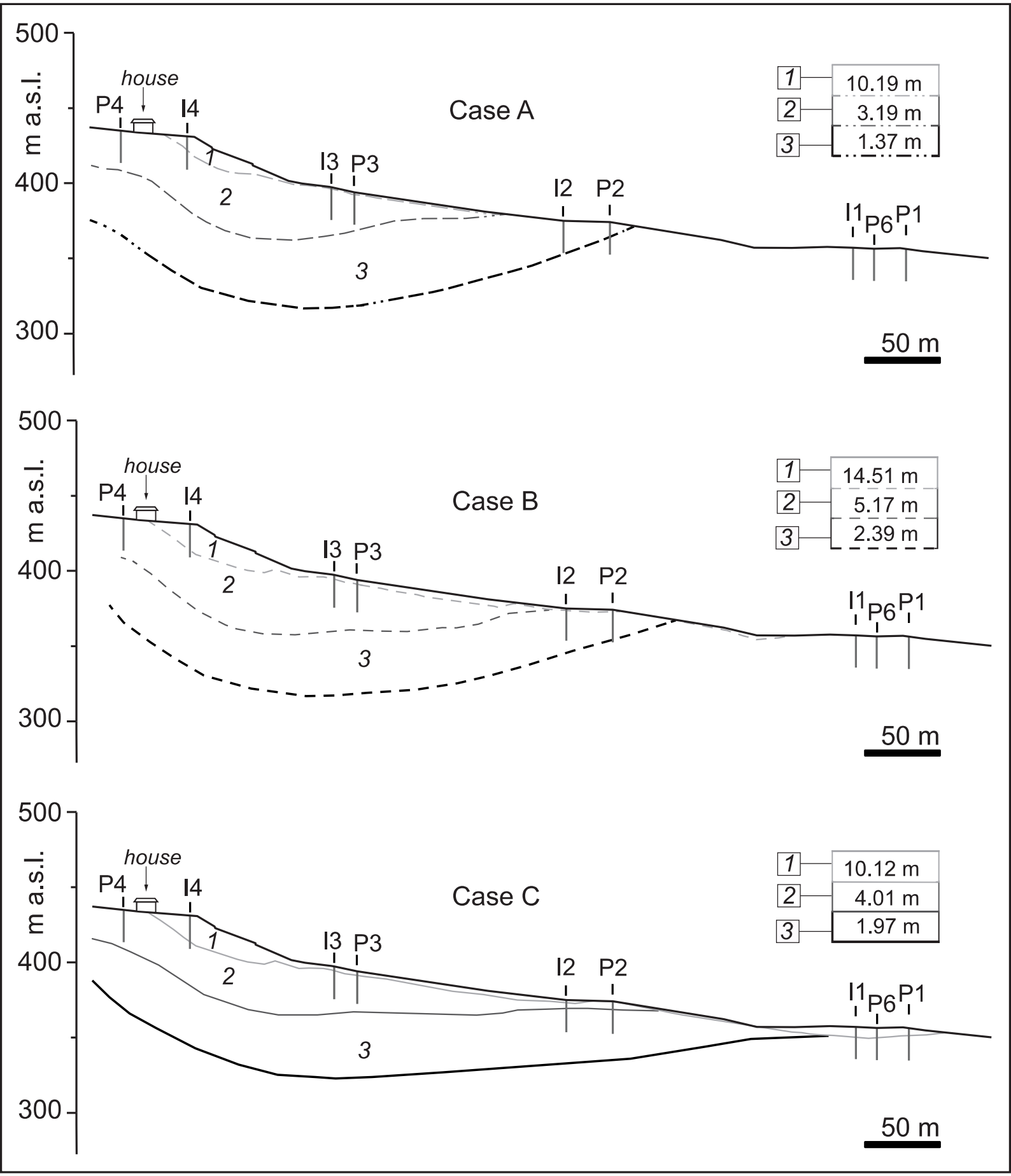


Fig. 17
Click here to download high resolution image

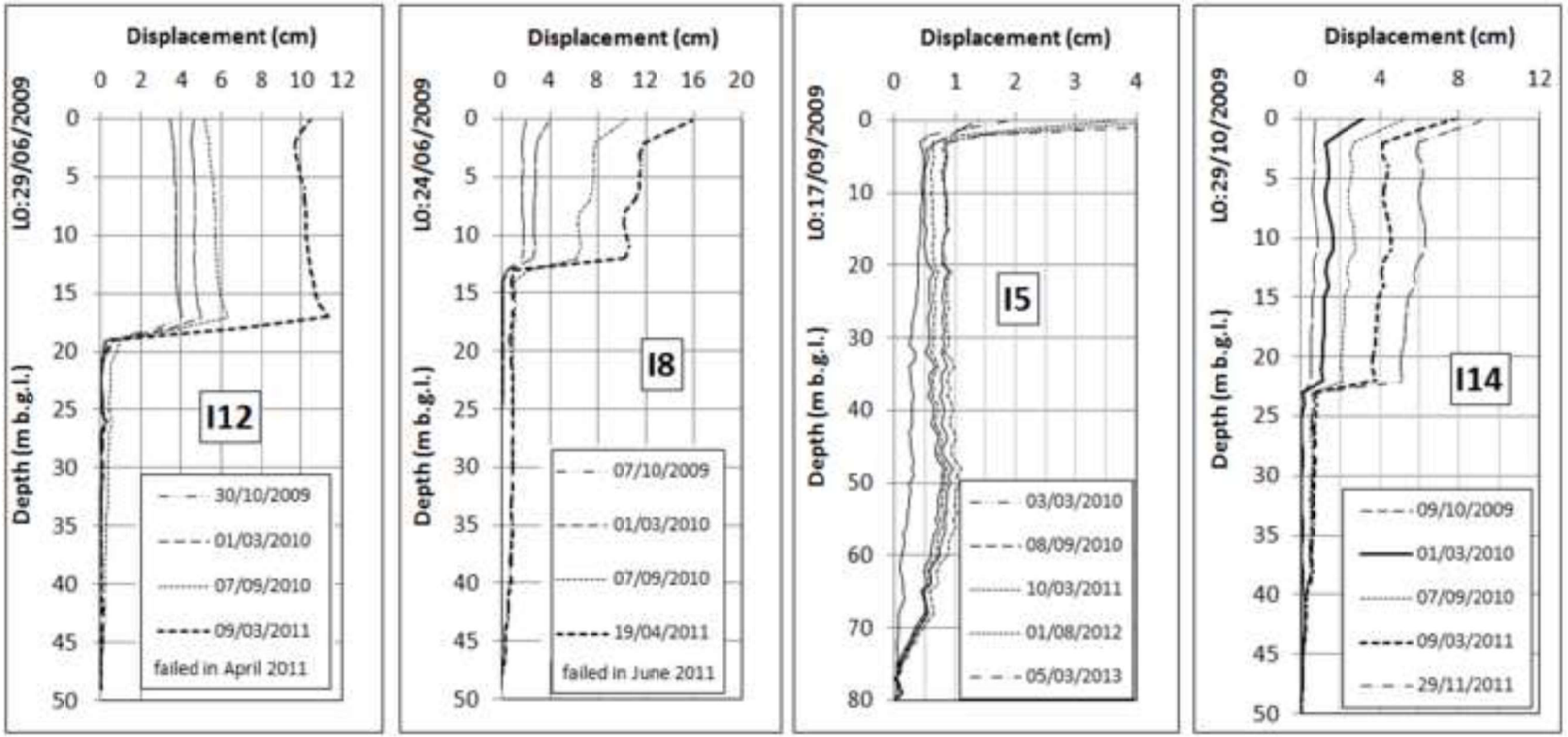


Fig. 18
Click here to download Figure: Fig18 Final.eps

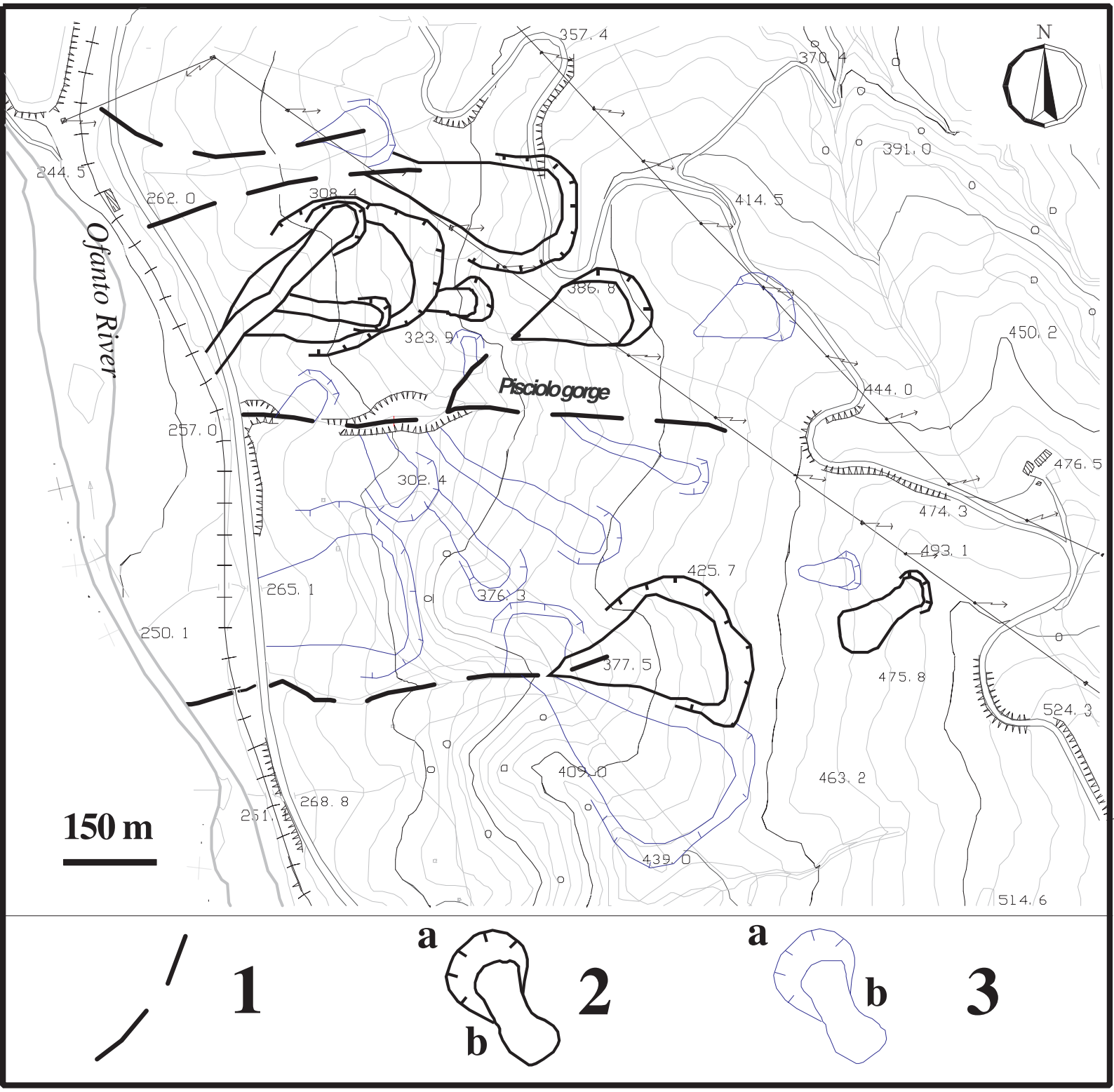


Fig. 19
Click here to download Figure: Fig19.eps

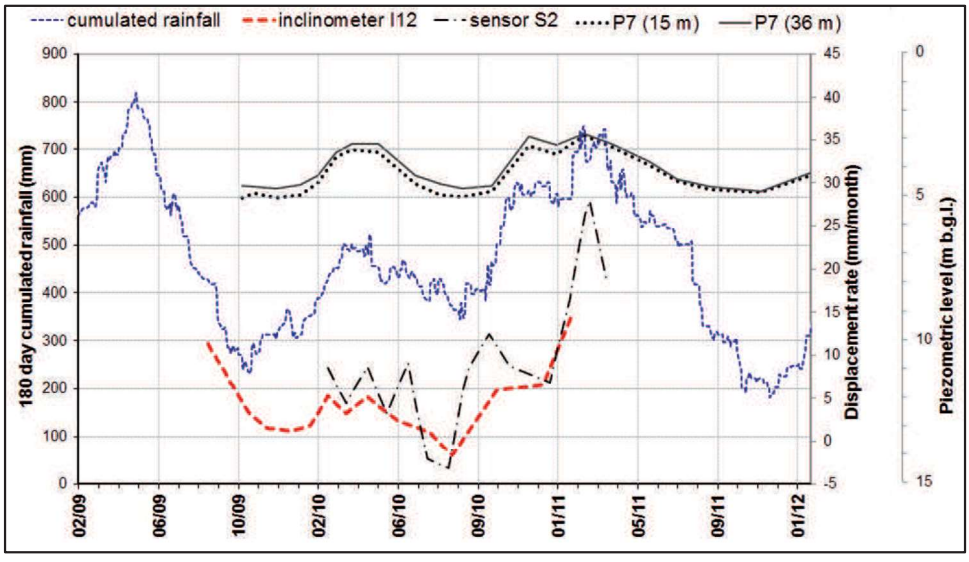


Fig. 20
Click here to download high resolution image

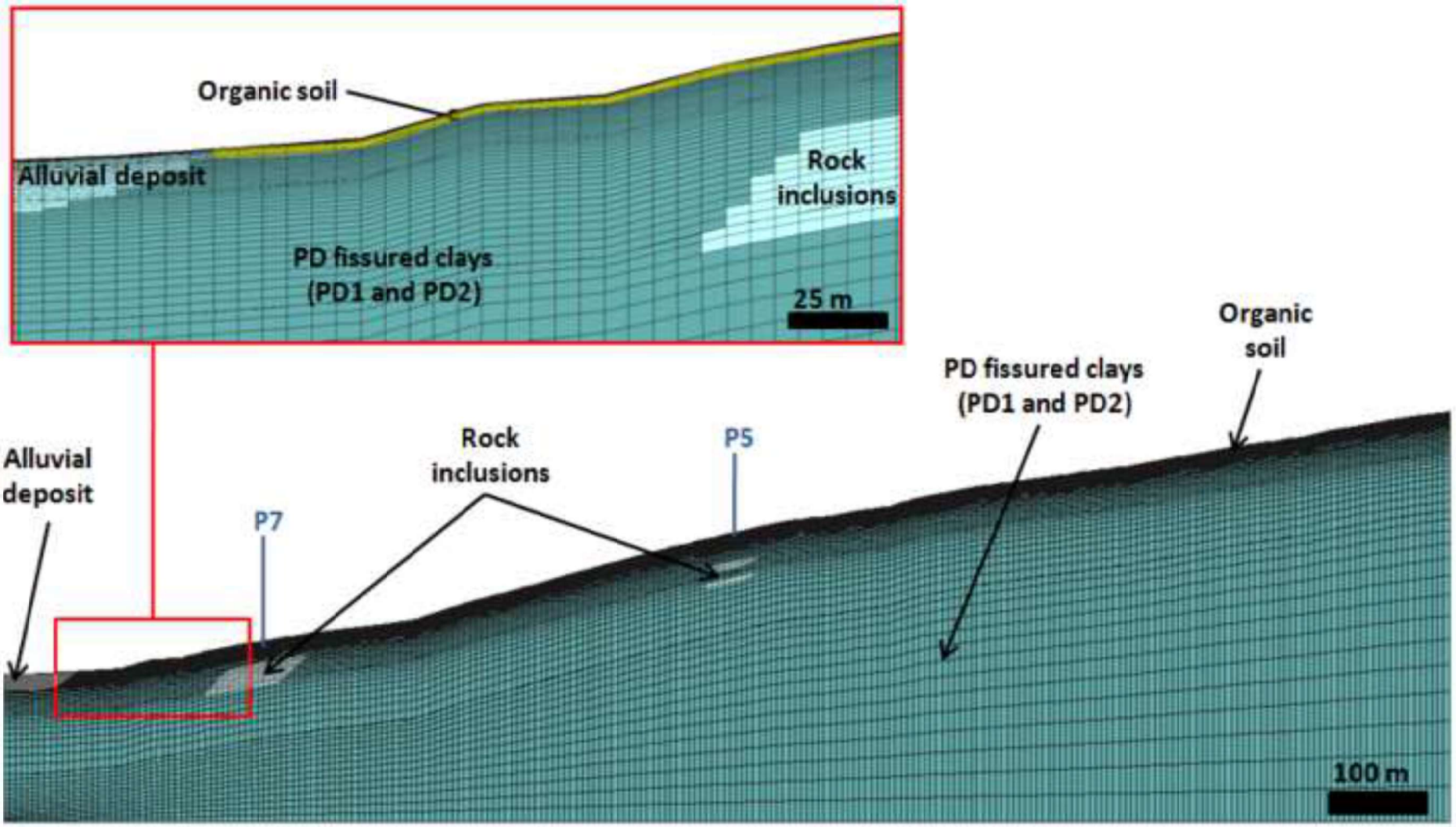


Fig. 21
Click here to download high resolution image

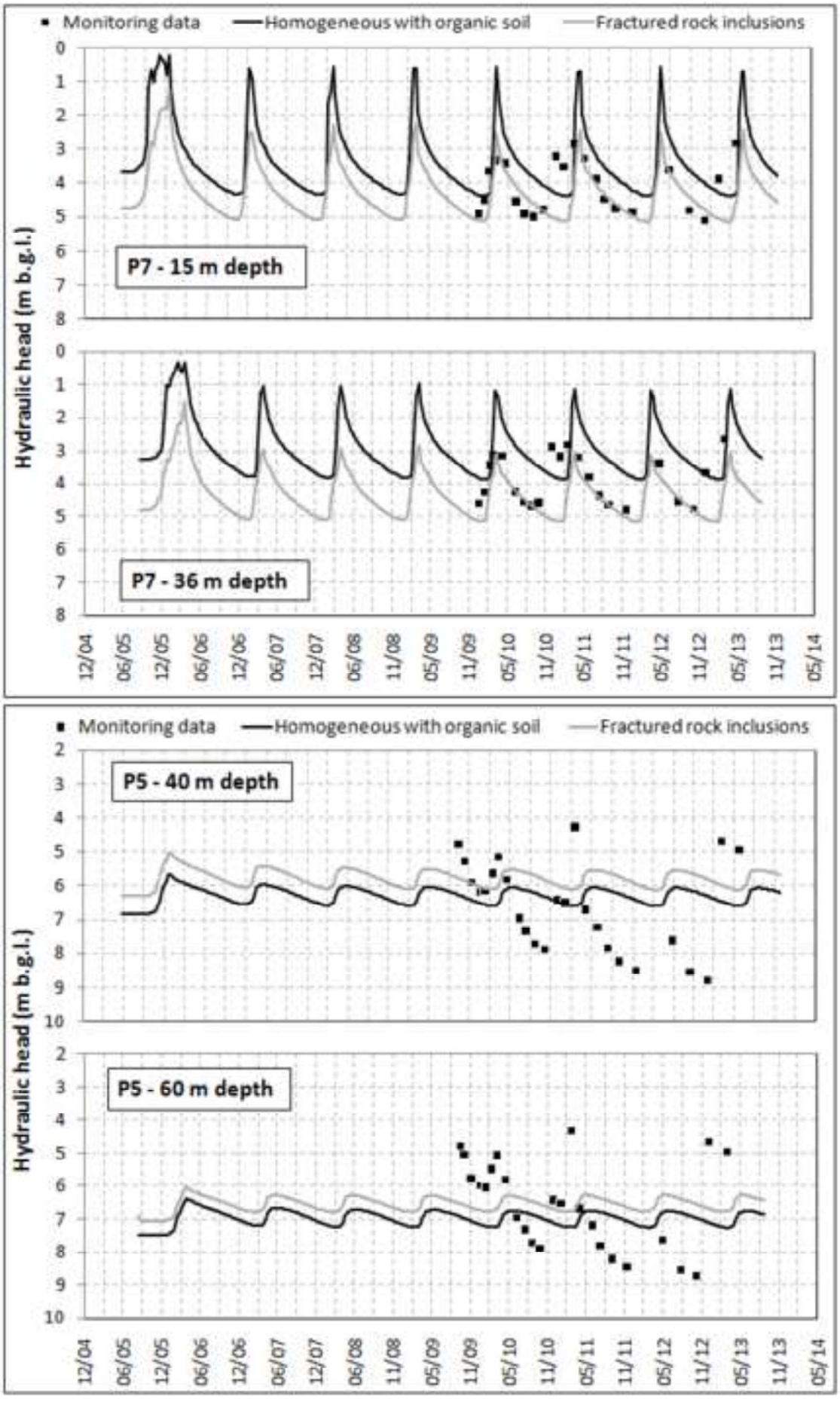


Table 1

Click here to download Table: Table 1.pdf

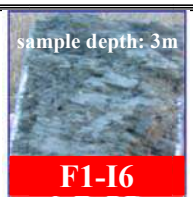
SLOPE	CLAY										
	Name	Fissuring characterisation *F-ID*	Sampling		Composition and physical properties						
			Type	Depth range (m b.g.l.)	CF %	SF %	PI %	A -	e_0 -	CI -	USCS Class
Santa Croce di Magliano (SCM)	SCM scaly clay	 **F1-I6** A1; B3-4; C3; D4-6; E1-3; F1; G1-4; H2; I6	block	3.0	91	9	55	0.6	0.88-1.05	1.1	CH
			borehole	54.4	73	-	28	0.4	0.54-0.64	1.9	CH
	BENT	 **F3-I5** A1; B4; C2-3; D4; E1-2; F3; G1, G4; H2; I5	block	18.0	66	2	86	1.3	1.55-1.79	0.9	CH
Vadoncello (SEN)	SEN scaly clay	 **F3-I6** A1; B2-3; C3; D4-6; E1-4; F3; G1-4; H2; I6	borehole	16.0-52.3	36-68	4-18	23-54	0.4-0.8	0.43-0.51	1.0-1.5	CH-CL
Pisciolo (PI)	PD2	 **F1-I5/I4** A1, A3; B3-4; C3; D6; E1-2; F1; G1; H1-2; I5/I4	borehole	6.0-80.0	19-55	16-26	24-44	0.5-1.0	0.41-0.69	1.0-1.6	CH
	PD1	 **F3-I6** A1, A3; B3-4; C3; D4, D6; E1-2; F3; G3-5; H2; I6		9.4-80.1	36-70	5-16	38-67	0.6-1.3	0.43-0.81	1.0-1.3	CH

Table 2

Click here to download Table: Table 2.pdf

SOIL TYPE	SHEAR TEST RESULTS
SE scaly clay	$\phi'_{peak} \approx 18.5°\text{-}20.5°$ (*dry* side, R≈ 3) – (a) $\phi'_{post\text{-}peak} = 12°\text{-}15°$ – (a) $\phi'_{r} \approx 5°$ – (b) $\phi^{*}_{cs} \approx 19°$ – (a)
SCM scaly clay	$\phi'_{peak} \approx 13°\text{-}22°$ (*dry* side, R≈ 2.5-20) – (a) $\phi'_{post\text{-}peak} = 9°\text{-}12°$ – (a) $\phi'_{r} \leq 9°$ – (c) $\phi^{*}_{cs} \approx 18°$ – (a)
BENT	$\phi'_{peak} \approx 16°\text{-}28°$ (*dry* side, R≈3-10) – (a) $\phi'_{post\text{-}peak} = 12°\text{-}27°$ – (a) $\phi'_{r} \approx 5°$ – (b) $\phi^{*}_{cs} \approx 16°$ – (a)
PD1and PD2 scaly clay	$\phi'_{peak} \approx 21°\text{-}25°$ (*dry* side, R≈3-10) – (a) $\phi'_{post\text{-}peak} = 13°\text{-}20°$ – (a) $\phi'_{r} \approx$ n.d. $\phi^{*}_{cs} \approx 18°$ – (a)